

1 **Projected future changes in cryosphere and hydrology of a mountainous**
2 **catchment in the Upper Heihe River, China**

3

4 Zehua Chang ¹, Hongkai Gao ^{1*}, Leilei Yong ¹, Kang Wang ¹, Rensheng Chen ²,
5 Chuntan Han ², Otgonbayar Demberel ³, Batsuren Dorjsuren ⁴, Shugui Hou ⁵, Zheng
6 Duan ⁶

7 ¹ Key Laboratory of Geographic Information Science (Ministry of Education of
8 China), School of Geographical Sciences, East China Normal University, Shanghai,
9 China

10 ² Qilian Alpine Ecology and Hydrology Research Station, Key Laboratory of
11 Ecohydrology of Inland River Basin, Northwest Institute of Eco-Environment and
12 Resources, Chinese Academy of Sciences, Lanzhou 730000, China

13 ³ Department of Geography and Geology Khovd branch of National University of
14 Mongolia, Erkh choolonii street, Khovd, Mongolia

15 ⁴ Department of Environment and Forest Engineering, National University of
16 Mongolia, Ulaanbaatar 210646, 84140, Mongolia

17 ⁵ School of Oceanography (SOO), Shanghai Jiao Tong University (SJTU), Shanghai,
18 China

19 ⁶ Department of Physical Geography and Ecosystem Science, Lund University,
20 Sölvegatan 12, SE-223 62, Lund, Sweden

21 *Correspondence: Hongkai Gao (hkgao@geo.ecnu.edu.cn)

22

23 **Abstract:** Climate warming exacerbates the degradation of the mountain cryosphere,
24 including glacier retreat, permafrost degradation and snow cover reduction. These

25 changes dramatically alter the local and downstream hydrological regime, posing
26 significant threats to basin-scale water resource management and sustainable
27 development. However, this issue is still not adequately addressed, particularly in
28 mountainous catchments. We developed an integrated cryospheric-hydrologic model,
29 FLEX-Cryo model, to comprehensively consider glaciers, snow cover, frozen soil, and
30 their dynamic impacts on hydrological processes. Taking the mountainous Hulu
31 catchment located in the Upper Heihe river of China as a case, we utilized the state-of-
32 the-art climate change projection data under two scenarios (SSP2-4.5 and SSP5-8.5)
33 from the sixth phase of the Coupled Model Intercomparison Project (CMIP6) to
34 simulate the future changes in the mountainous cryosphere and their impacts on
35 hydrology. Our findings showed that under the medium (SSP2-4.5) and high emission
36 scenario (SSP5-8.5), by the end of the 21st century, the glacier will completely melt out
37 around the years 2051 and 2045, respectively. The annual maximum snow water
38 equivalent is projected to decrease by 41.4% and 46.0%, while the duration of snow
39 cover will be reduced by approximately 45 and 70 days. The freeze onset of seasonally
40 frozen soil is expected to be delayed by 10 and 22 days, while the thaw onset of
41 permafrost is likely to advance by 19 and 32 days. Moreover, the maximum freeze depth
42 of seasonally frozen soil is projected to decrease by 5.2 and 10.9 cm per decade, and
43 the depth of the active layer will increase by 8.2 and 15.5 cm per decade. Regarding
44 hydrology, catchment total runoff exhibits a decreasing trend and the tipping point of
45 glacier runoff occur approximately between 2019 and 2021. Permafrost degradation
46 will likely reduce the duration of low runoff in the early thawing season, the
47 discontinuous baseflow recession gradually transitions into linear recessions and the
48 increase of baseflow. Our results highlight the significant changes expected in the

49 mountainous cryosphere and hydrology in the future. These findings enhance our
50 understanding of cold-region hydrological processes and have the potential to assist
51 local and downstream water resource management in addressing the challenges posed
52 by climate change.

53 **Keywords:** Glacier, Snow cover, Seasonally frozen soil, Permafrost, Runoff, Model
54 prediction

55 1. Introduction

56 “How will cold region runoff and groundwater change in a warmer climate?” was
57 identified by the International Association of Hydrological Sciences (IAHS) as one of
58 the 23 unsolved scientific problems (Blöschl et al., 2019). The mountain cryosphere,
59 which includes glaciers, snow cover, and frozen soil in high-altitude regions, has a
60 significant impact on water resources (Adler et al., 2019; Arendt et al., 2020; Rasul et
61 al., 2020; Zhang et al., 2022). The mountain cryosphere is considered a crucial "water
62 tower" and a climate change indicator due to its sensitivity to climate change (Tang et
63 al., 2023). However, the cryosphere is rapidly retreating in many parts of the world,
64 including glacier retreat, expansion of glacier lakes, northward movement of the
65 permafrost southern limit, and shrinking snow cover area (Moreno et al., 2022; S. Wang
66 et al., 2022; Ding et al., 2019; Wang et al., 2023). These changes have disrupted the
67 water tower region and pose significant challenges to sustainable water resources
68 management (Ragettli et al., 2016; Yao et al., 2022).

69 The degradation of the mountain cryosphere varies from region to region
70 (Andrianaki et al., 2019; Wang et al., 2019). Lower altitudes experience a decreasing
71 trend in snow cover days, snow depth, snow water equivalent, and snowmelt due to
72 climate warming, while higher altitudes present a more complex picture (Connon et al.,

73 2021; Nury et al., 2022; Yang et al., 2022). Global continental glacier mass balance
74 from 2006 to 2015 was approximately -123 ± 24 GT yr⁻¹, with significant losses
75 observed in the Southern Andes, Caucasus Mountains, and Central Europe, while the
76 Karakoram and Pamir regions exhibited lesser loss (Intergovernmental Panel on
77 Climate Change (IPCC), 2022; Van Der Geest and Van Den Berg, 2021). Future
78 projections suggest a 40% decrease in global permafrost by the end of the century,
79 potentially transitioning into seasonally frozen soil (Chadburn et al., 2017; Martin et al.,
80 2023). The mountain cryosphere serves as a significant freshwater reservoir, impacting
81 water resources and the hydrological cycle (Ding et al., 2020).

82 In a warming climate, glacier runoff exhibits a "tipping point" characterized by an
83 initial increase followed by a subsequent decline (Rosier et al., 2021; Zhang et al., 2012).
84 While small glaciers have already experienced this tipping point, its occurrence in large
85 glaciers remains uncertain (Brovkin et al., 2021; Huss and Hock, 2018). Permafrost
86 degradation leads to an increase in active layer thickness, resulting in the melting of
87 subsurface ice and an augmentation of soil water storage capacity (Abdelhamed et al.,
88 2022). Additionally, the degradation of the cryosphere significantly impacts the
89 atmosphere, biosphere, surface energy balance, ecological water use, and ecosystems
90 (Gilg et al., 2012; Miner et al., 2022; Pothula and Adams, 2022). Understanding the
91 complex interactions between cryosphere degradation and ecosystems is crucial, but
92 quantitatively observing the degradation process in high-altitude regions is challenging.
93 Hydrological models provide an effective approach to analyze degradation patterns and
94 assess the impact on future water resources (Han and Menzel, 2022).

95 Glacio-hydrology is influenced by both glacier melt and glacier dynamics. Glacier
96 melting models can be categorized into three types: energy balance, temperature index,

97 and hybrid models (He et al., 2021; Gao et al., 2021; Negi et al., 2022; Zekollari et al.,
98 2022). While energy balance models analyze glacier accumulation and melt processes
99 based on solid physical mechanisms, they require extensive forcing data that may not
100 be readily available in mountainous regions (Huss et al., 2010). In contrast, temperature
101 index models are simpler and more effective, requiring fewer parameters (including
102 degree-day factor and threshold temperature) and forcing data (temperature and
103 precipitation) (Bolibar et al., 2022; Vincent and Thibert, 2023). These models perform
104 well at both daily and monthly scales. Glaciers move slowly due to the combined effects
105 of gravity and high viscosity of ice. Due to climate change, ice becomes thinner, and
106 glacier loses its mass balance, which will cause the glacier morphology to evolve to a
107 new balance status. Glacier dynamic models, with full-Stokes approach as the most
108 complete form, and many other simplifications, such as the shallow-ice approximation,
109 and the shallow-shelf approximation, are still computationally expensive, hindering
110 their implications in large scale studies. Three conceptual models are commonly used
111 for glacier evolution: volume-area scaling (V-A) method, accumulation area ratio (AAR)
112 method, and Δh -parameterization (Michel et al., 2022; Wiersma et al., 2022). The first
113 two approaches do not consider the detailed changes in different elevation bands, while
114 the Δh -parameterization approaches only require glacier mass balance as forcing data
115 to analyze changes in ice thickness at different elevation bands based on the relationship
116 between glacier mass balance and glacier area (Huss et al., 2010). The temperature
117 index method coupled with the Δh -parameterization approach serves as an effective
118 module to simulate glacier evolution and its impacts on hydrology.

119 Permafrost hydrology models can be classified into one-dimensional models and
120 distributed watershed models (Elshamy et al., 2020). One-dimensional hydrological

121 models, such as the Stefan equation, the temperature at the top of permafrost (TTOP)
122 model, CoupModel, and SHAW model, are effective in simulating freeze depth,
123 hydrothermal transport, and carbon or nitrogen transport, but they are unable to capture
124 the broader impact of permafrost on hydrology at catchment scale (Kaplan Pastíriková
125 et al., 2023; Li et al., 2022; Liu et al., 2023). On the other hand, distributed watershed
126 models, such as the Cold Regions Hydrological Model (CRHM), Hydrogeosphere
127 (HGS), and Distributed water-heat coupled model (DWHC), consider the spatial
128 variability of permafrost properties and simulate the interactions between permafrost,
129 surface water, and groundwater (Chen et al., 2008; He et al., 2023; Pomeroy et al.,
130 2022). These models operate on a small-scale basis and require extensive prior
131 knowledge, following a "bottom-up" approach that relies on small-scale field
132 observations and situational models to comprehend the effects of permafrost on
133 hydrology (Peng et al., 2016). However, the freeze-thaw cycle is influenced by multiple
134 interconnected factors, including climate, topography, slope orientation, snowpack, and
135 vegetation (Chang et al., 2022). The process of upscaling would lead to the neglect of
136 some variables and the amplification of others (Fenicia and McDonnell, 2022). In
137 contrast, the FLEX-Cryo model is based on the FLEX-Topo-FS model, which employs
138 a "top-down" modeling procedure that involves observed data analysis, qualitative
139 perceptual modeling, quantitative conceptual modeling, and the testing of model
140 realism. This model exhibits the ability to accurately and expeditiously identify key
141 elements in permafrost hydrological processes and then simulate hydrology at the
142 catchment scale (Beven., 2012; Gao et al., 2022).

143 The aim of this study is to integrate the FLEX-Topo-FS model and a glacier
144 evolution model (Δh -parameterization) to develop a landscape-based model of the

145 mountain cryosphere, referred to as FLEX-Cryo. This model will be utilized to simulate
146 changes in various components of the mountain cryosphere and evaluate their impacts
147 on hydrological processes, thereby enhancing our understanding of the hydrological
148 cycle. The model will be driven by eight bias-corrected Global Climate Models (GCMs)
149 under SSP2-4.5 and SSP5-8.5 scenarios obtained from the Coupled Model
150 Intercomparison Project Phase 6 (CMIP6), which will be used to predict future changes
151 in glaciers, snow, and frozen soil, as well as their effects on hydrology.

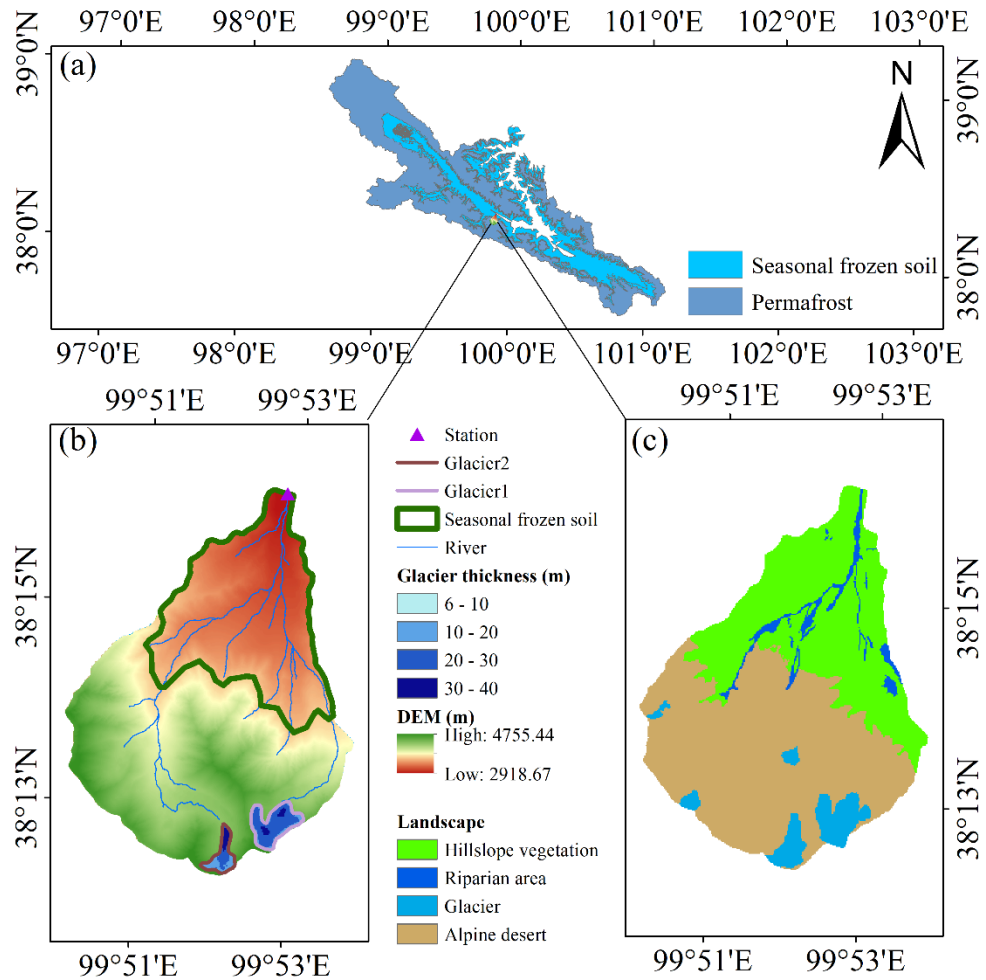
152 **2.Study area and data**

153 **2.1 Study area**

154 The Hulu catchment is located in the upper reaches of Heihe River basin ($38^{\circ} 12'$
155 $N-38^{\circ} 17' N$, $99^{\circ} 50' E-99^{\circ} 53' E$) and about 23.1 km^2 . The elevation ranges
156 from 2960-4820m. The Hulu catchment belongs to continental monsoon climate.
157 Rainfall is the major phase of precipitation, and there is also snowfall in the winter.
158 Four landscapes are identified, i.e. glacier (5.6%), alpine desert (53.5%), vegetation
159 hillslope (37.5%), and riparian zone (3.4%; Fig.1 (c)). The landscape pattern in Hulu
160 catchment has typical altitude zonality. The vegetation and riparian are almost
161 distributed in the lower elevation bands. Alpine desert, and glacier are in the high
162 elevation bands. There is almost no human activity in the catchment (Liu and Chen,
163 2016; Li et al., 2014). There are two major glaciers, i.e. Glacier1 and Glacier2 (Fig.1
164 (b) and Fig.2) in the catchment. And the Glacier1 was also named as the Shiyi Glacier
165 in the glacier catalogue of China. Seasonally frozen soil and permafrost both exist in
166 the catchment. The lower limit of permafrost is around in 3650-3700 m. Permafrost
167 region account for 64% of the total catchment and the others are seasonally frozen soil.
168 The soil generally starts to freeze in the October (Gao et al., 2019). Thus October 1 was

169 set as the start of hydrological year, so forth. All the interannual variations in this study
 170 were based on the hydrology year.

171

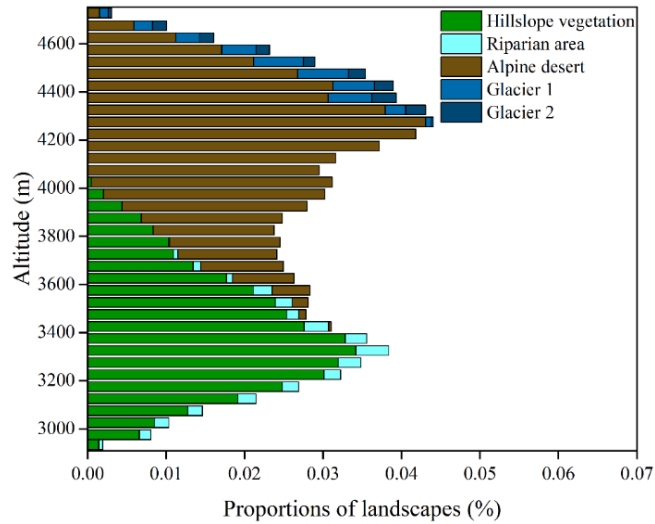


172

173 Figure 1. (a) The distribution of permafrost and seasonally frozen soil on the
 174 upper Heihe River basin, and the location of Hulu catchment. (b) The digital elevation

175 model and the thickness of the two major glaciers. (c) Spatial distribution of four

176 landscapes (glacier, alpine desert, vegetation hillslope, and riparian zone)



177

178

Figure 2. Landscape classification at different elevation bands

179 **2.2 Data**

180 Temperature and precipitation are observed at 2920 m, near the outlet of the
 181 catchment, from 2011 to 2014. Farinotti et al. (2019) used five models which used the
 182 ice flow dynamics to invert ice thickness from surface features to estimate the ice
 183 thickness distribution of about 21500 glaciers outside the Greenland and Antarctic ice
 184 sheets. We used the estimated data for the initial thickness distribution of Glacier1 and
 185 Glacier2 (data downloaded from <https://doi.org/10.3929/ethz-b-000315707>).

186 The Couple Model Intercomparison Project phase 6 (CMIP6) is widely used to
 187 predict future climate. Eight general circulation models (GCMs) (Table 1) under two
 188 climate scenarios (SSP2-4.5 and SSP5-8.5) are used for predicting future climate. The
 189 selected models have been well validated at the nearby catchments (Xing et al., 2023;
 190 Yin et al., 2021; Ma et al., 2022; Zhu and Yang, 2020; Chen et al., 2022). SSP2-4.5
 191 scenario represents medium part of the future pathways, which is usually a referenced
 192 experiment comparing others CMIP6-Endorsed MIPs and it produces a radiative
 193 forcing of 4.5 W m⁻² in 2100. SSP5-8.5 scenario represents the high emission scenario
 194 and it produce a radiative forcing of 8.5 W m⁻² in 2100.

195 Although the reliability of GCMs has been verified in the previous studies, there
 196 is certain bias in the output that needs to be corrected. Firstly, outputs from eight GCMs
 197 under two climate scenarios are interpolated to $0.5^{\circ} \times 0.5^{\circ}$, then the bias corrects are
 198 carried out by CMhyd software (download from
 199 <https://swat.tamu.edu/software/cmhyd/>) in which four methods were used including:
 200 distribution mapping of precipitation and temperature, linear scaling of precipitation
 201 and temperature, variance scaling of temperature and local intensity scaling (LOCI) of
 202 precipitation (Teutschbein and Seibert, 2012). The bias-corrected precipitation and
 203 temperature were calculated by using the equal weighted average method to obtain the
 204 multi-model ensemble average values under the SSP2-4.5 and SSP5-8.5 scenarios,
 205 which reduce the uncertainty caused by a single bias correction method and a single
 206 GCM, the method is described as follow:

$$207 \quad P_{ave} = \frac{1}{N_{GCM}} \left(\sum_{j=1}^{N_{GCM}} \left(\frac{1}{N_{bias}} \left(\sum_{i=1}^{N_{bias}} (P_i) \right) \right) \right) \quad (1)$$

208 Where the P_{ave} is the average value of the multi-model and multi -method, P_i is the
 209 projected climate data of an GCM, N_{bias} is the number of correction methods (N_{bias} is 3
 210 in this research) and N_{GCM} is the number of GCM (N_{GCM} is 8 in this research).

211 Table 1. Details of data from eight GCMs used in this study

GCM	Institutions	Grid	Lon. × Lat.
ACCESS-CM2	Australian Community Climate and Earth System Simulator	192×144	1.875°×1.250°
ACCESS-ESM1-5	Australian Community Climate and Earth System Simulator	192×144	1.875°×1.250°
BCC-ECM1	Beijing climate center	320×160	1.125°×1.125°
CMCC-CM2-SR5	Fondazione Centro Euro-	288×192	1.25°×0.938°

	Mediterraneo sui Cambiamenti Climatici Fondazione Centro Euro- Mediterraneo sui Cambiamenti Climatici,	288×192	1.25°×0.938°
CMCC-ESM2	National Oceanic and Atmospheric Administration	144×90	2.5°×2°
GFDL-CM4	Max Planck Institute for Meteorology	192×96	1.875°×1.875°
MPI-ESM1-2-LR	Nanjing University of Information Science and Technology	192×96	1.875°×1.875°
NESM3			

212 3.Methodology

213 3.1 FLEX-Cryo model

214 The FLEX-Cryo model is a landscape-based cryospheric hydrological model that
215 considers multiple elements of cryosphere and their impacts on hydrology, including
216 glacier, snow and frozen soil. Figure 3 shows the structure of the FLEX-Cryo model.

217 The model parameters used in this research were obtained the optimal parameter
218 set from a previous study conducted in the same catchment (Gao et al., 2022). The
219 selected parameters are listed in Table 2 and the other variables in calculating (Fig. 3)
220 are listed in Table 4.

221 Table 2. Model parameters and their values in this study

Parameter	Name	Parameter value
F_{dd} ($\text{mm}^{\circ}\text{C}^{-1}\text{d}^{-1}$)	Snow degree day factor	3.10
C_g (-)	Glacier degree factor multiplier	2.27
$S_{\text{umax_V}}$ (mm)	Root zone storage in vegetation hillslope	100.32
$S_{\text{umax_D}}$ (mm)	Root zone storage in alpine desert	20.63
$S_{\text{umax_R}}$ (mm)	Root zone storage in riparian wetland	20.26
β (-)	The shape of storage capacity curve	0.11

C_e (-)	Soil moisture threshold for reduction of evaporation	0.50
D (-)	Splitter to fast and slow response reservoirs	0.20
T_{lagf} (days)	Lag time from rainfall to peak flow	2.00
K_f (days)	Fast recession coefficient	1.65
K_s (days)	Slow recession coefficient	79.09
k (W (m K) ⁻¹)	Thermal conductivity	2.00
ω (-)	Water content as a decimal fraction of the dry soil weight	0.12
ρ (kg/m ³)	Bulk density of the soil	1000
P_{calt} (%/100m)	Precipitation increasing rate	4.20
T_{calt} (°C/100m)	Temperature lapse rate	0.68

222 3.1.1 Glacier and snow melting

223 The threshold temperature (T_l) determines the phase of precipitation, i.e. snowfall
224 or rainfall. Snow reservoir (S_w) accounts for the snow accumulating, melting (M_w) and
225 water balance(Eq. 9). The number of days when S_w is non-zero represent the snow cover
226 days and the maximum S_w is the maximum snow water equivalent of a year (Giovando,
227 J. and Niemann, J. D., 2022). Both Glacier and snow melt were calculated by the
228 temperature index method, which is on basis of the degree-day factor (F_{dd}). If there is
229 no s'ow cover, the glacier starts to melt. Due to the lower albedo, the degree-day factor
230 of ice is greater than that of snow cover, and is multiplied by a coefficient C_g to calculate
231 glacier melt (Eq. 14).

232 3.1.2 Rainfall-runoff module

233 The rainfall and snow melt enter the root zone reservoir S_u , then runoff (R_U)
234 generates based on the input water and the relative root zone soil moisture (S_u/S_{umax})
235 and the shape of root zone storage capacity distribution determined by parameter β (Eq.
236 16). Actual evaporation E_a is also estimated based on the soil moisture S_u/S_{umax} and the

237 potential evaporation by Hamon equation (Hamon, 1961). The generated runoff (R_U) is
 238 separated, by parameter D , into two linear reservoirs, i.e. the fast response reservoir (S_f)
 239 and slow response reservoir (S_s) (Eq. 18 and 19). The two reservoirs are respectively
 240 controlled by fast recession parameter K_f and slow recession parameter K_s to simulate
 241 the subsurface storm flow Q_f and groundwater runoff Q_s (Eq. 7,8).

242 Different landscapes, for example, alpine desert, vegetation hillslope and riparian
 243 zone, have different sizes of root zone storage capacity (S_{umax}) (Aubry-Wake et al.,
 244 2023). In the vegetation hillslope, plants have well-developed root systems and the root
 245 zone has a larger storage capacity. Therefore, the S_{umax_V} was set to a larger value. For
 246 the alpine desert and riparian zone, the S_{umax_D} and S_{umax_R} were both limited due to the
 247 less developed root system and storage capacity.

248 **3.2 Frozen soil module**

249 The Stefan equation was employed to estimate freeze (thaw) depth. This equation
 250 is calculated by the freeze (thaw) index (F), which neglects the sensible heat. The
 251 equation is as follows:

$$252 \quad \varepsilon = \left(\frac{2 \cdot 86400 \cdot k \cdot F}{L \cdot \omega \cdot \rho} \right)^{0.5} \quad (2)$$

253 where, the ε is the freeze / thaw depth (m), k is the thermal conductivity (2 W (m
 254 K)⁻¹), F is the freeze/ thaw index(°C), Q_L is the volumetric latent heat of soil (J m⁻³), L
 255 is the latent heat of the fusion of ice (3.35×10^5 J kg⁻¹), ω is the water content as a
 256 decimal fraction of the dry soil weight (0.12), and ρ is the bulk density of the soil
 257 (1000 kg m⁻³).

258 Since the Stefan equation requires ground surface temperature, which is difficult
 259 to measure and often lacks data. During freezing, the air temperature was translated into
 260 ground temperature by multiplier 0.6 and the ground temperature was the same as the

261 air temperature during thawing (Gisnås et al., 2016). In this research, the freeze-thaw
262 process was simulated at each Hydrologic Response Unit (RHU) by the Stefan equation
263 driven by distributed air temperature. The lower limit of permafrost was also estimated
264 by the distributed soil freeze index and thaw index where the freeze index is equal to
265 the thaw index in the mountain region.

266 In the freezing and frozen season, there is no runoff generated due to precipitation
267 in the form of snowfall and the soil being frozen. During this period, runoff only comes
268 from the groundwater of the supra-permafrost and no runoff (R_U) is generated from root
269 zone reservoir to the fast response reservoir (S_f) and slow response reservoir (S_s).
270 Therefore, we set the R_U is zero in this season. In the freezing season, when the freezing
271 depth is less than 3 m, the groundwater discharge in the supra-permafrost is still
272 connected, which can be simulated with a linear groundwater reservoir (S_s) and the slow
273 recession coefficient (K_s). When the freezing depth is greater than 3 m at a Hydrologic
274 Response Unit, the groundwater is frozen and there is little runoff generated from the
275 groundwater discharge at the Hydrologic Response Unit. So, in the FLEX-Cryo model,
276 the groundwater reservoir (S_s) was reduced to 10% of its storage to represent the
277 groundwater being frozen (Eq. 3,4). The other 90% of the storage water was frozen in
278 the groundwater system (Eq. 4). In the model, the soil begins to freeze from high
279 elevation to the lower elevation, which affects the groundwater. The groundwater
280 reservoir freezes along the elevation, stopping the function of a series of cascade
281 groundwater buckets, which is the key reason for discontinue recession.

282 In the thawing season, the freeze statue at the lowest elevation controls the
283 hydraulic connectivity between groundwater system and soil. If the freeze depth is
284 larger than thaw depth calculated by the Stefan equation, the soil is still frozen and the

285 connectivity between groundwater system and soil is still closed. There is no runoff
 286 generated (Ru) but the root soil moisture (Su) accumulates and evaporation is the only
 287 outflow from the root zone. Once the thaw depth is larger than the freeze depth, the
 288 frozen groundwater reservoir is released to the groundwater discharge (Eq. 4).
 289 Complete thawing at the lowest elevation represents the end of the thawing season and
 290 the start of completely thawed season. In the completely thawed season, the
 291 groundwater and soil are connected and not affected by the frozen soil.

$$292 \quad \frac{dS_s}{dt} = R_s - Q_s - F_s \quad (3)$$

$$293 \quad F_s = \begin{cases} 0.9 \cdot S_s & \text{freeze depth } (\varepsilon) \geq 3 \text{ m} \\ -0.9 \cdot S_s & \text{once thaw depth reach to yearly max} \\ & \text{or thaw depth } \geq \text{thaw depth} \end{cases} \quad (4)$$

294 3.3 Δh -parameterization

295 The Δh -parameterization is a mass conservation method to assess the change of
 296 ice-covered, glacier length and glacier thickness in response to global warming. The
 297 glacier mass balance (GMB) calculated by FLEX-Cryo was redistributed to glacier
 298 elevation bands. It is an observed truth that the lower elevation bands loss more ice than
 299 higher elevation bands. The lost ice volume, calculated by a mass balance model, is
 300 converted into a distributed ice thickness change according to the Δh -parameterization.
 301 (Gao et al., 2021; Huss et al., 2010).

302 The Δh -parameterization method was employed, which relies on empirical curves
 303 that are dependent on the size of the glacier. The study categorized glaciers into three
 304 size classes: large valley glacier (area $> 20 \text{ km}^2$), medium valley glaciers ($5 \text{ km}^2 < \text{area}$
 305 $< 20 \text{ km}^2$), and small glaciers (area $< 5 \text{ km}^2$). Both Glacier1 and Glacier2 had areas less
 306 than 5 km^2 , and categorized as small glaciers. The small glacier equation in this study
 307 is as follows:

308
$$\Delta h = (h_r - 0.30)^2 + 0.60(h_r - 0.30) + 0.09 \quad (5)$$

309 Where, Δh is normalized surface elevation change and h_r is the normalized
 310 elevation range. Based on this equation, the glacier elevation and surface area were
 311 evolved every 5 years to avoid the circumstance of glacier advancing. The
 312 corresponding glacier melting HRU was transformed into alpine desert (Wei et al.,
 313 2023).

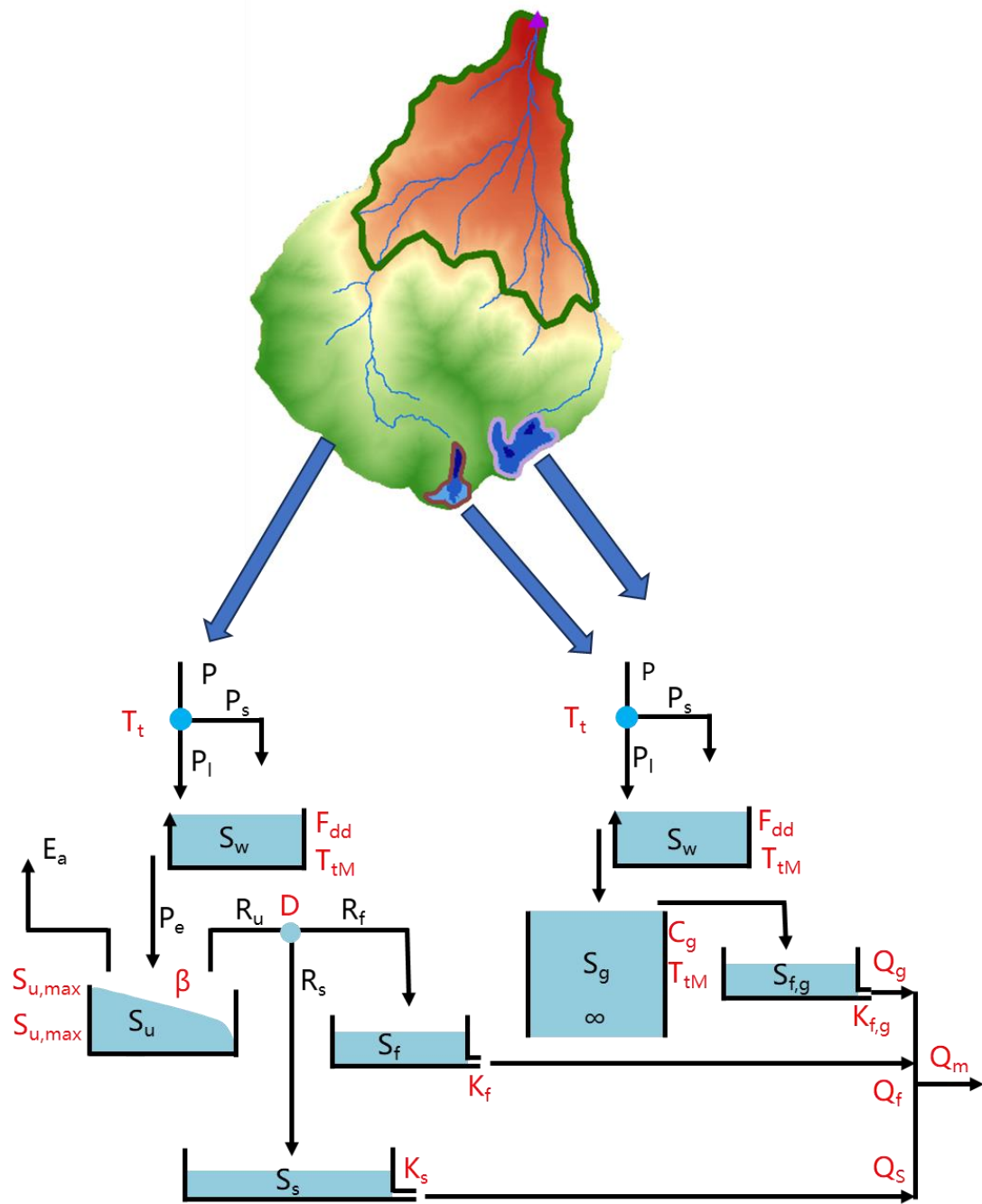
314

315 Table 3. The FLEX-Cryo model equations

Landscape	Runoff equation	Water balance equation	Structural equation
Glacier	$Q_g = \frac{S_g}{K_{f,g}} \quad (6)$	$\frac{dS_g}{dt} = P_l + M_g - Q_g \quad (9)$	$M_g = \begin{cases} F_{dd} \cdot T \cdot C_g & S_w \text{ and } T > 0 \\ 0 & S_w \text{ and } T < 0 \end{cases} \quad (14)$
Alpine desert		$\frac{dS_w}{dt} = P - M_w \quad (10)$	$M_w = \begin{cases} F_{dd} \cdot T & T > 0 \\ 0 & T < 0 \end{cases} \quad (15)$
Hillslope vegetation	$Q_f = \frac{S_f}{K_f} \quad (7)$	$\frac{dS_u}{dt} = P_l + M_w - E_a - R_u \quad (10)$	$R_u = (P_l + M_w) \cdot \left(1 - \left(1 - \frac{S_u}{S_{u\max}}\right)^\beta\right) \quad (16)$
			$E_a = E_p \cdot \left(\frac{S_u}{C_e \cdot S_{u\max}}\right) \quad (17)$
			$R_f = R_u \cdot D \quad (18)$
		$\frac{dS_f}{dt} = R_f - Q_f \quad (12)$	$R_s = R_u \cdot (1 - D) \quad (19)$
Riparian area	$Q_s = \frac{S_s}{K_s} \quad (8)$	$\frac{dS_s}{dt} = R_s - Q_s \quad (13)$	$R_{f,t}(t) = \sum_{i=1}^{T_{lagf}} cf(i) \cdot R_f(t - i + 1) \quad (20)$
			$cf(i) = i / \sum_{u=1}^{T_{lagf}} u \quad (21)$

316 **3.4 Spatial discretization of the catchment**

317 The catchment area was divided into 37 elevation bands ranging from 2960 m to
318 4820 m, with an interval of 50 m. These elevation bands were classified based on four
319 landscapes: glacier, alpine desert, vegetation hillslope, and riparian zone (Fig. 2 and Fig.
320 3). As a result, there were a total of 148 Hydrologic Response Units (HRUs) in the
321 catchment. The landscape of alpine desert was the most widespread, covering an
322 elevation range of 3425 m to 4727 m. The glacier was found in higher altitude areas,
323 specifically between the elevation bands of 3725 m and 4727 m.



324

325 Figure.3 Structure of the FLEX-Cryo model. The abbreviation in red color indicates

326 parameters and the abbreviations in black indicate storage components and fluxes.

327 Table 4. The variables in Table 3 and Figure 3 and their meaning

Variables	Meaning
P (mm/day)	precipitation
T_t ($^{\circ}\text{C}$)	Threshold temperature
P_s (mm/day)	Solid precipitation

P_l (mm/day)	Liquid precipitation
S_{wl} (mm)	Liquid water inside the snow pack.
S_w (mm)	Solid snow pack
T_{tM} (°C)	The threshold temperature for snow and glaciers melting
P_e (mm)	Generated runoff to soil/ice surface
E_a (mm)	Actual evaporation
R_u (mm)	water that exceeds the storage capacity
S_f (mm)	Fast flow reservoir
S_s (mm)	Slow flow reservoir
$S_{f,g}$ (mm)	Glacier linear reservoir
Q_f (mm/day)	Subsurface storm flow
Q_s (mm/day)	Groundwater runoff
Q_g (mm/day)	Runoff in glacier region
Q_m (mm/day)	All runoff

328 3.5 Model evaluation metrics

329 The Kling–Gupta efficiency (KGE), Nash–Sutcliffe efficiency (NSE), coefficient
330 of correlation (R) and root mean square error (RMSE) were used to comprehensively
331 assess the model performance and the reliability for the model. All The KGE, NSE, R
332 and RMSE are all less than 1. For KGE, NSE and R, values closer to 1 indicate better
333 performance. A lower RMSE value indicates less error and better model performance.

334 These metrics can be calculated as follows:

335
$$KGE = 1 - \sqrt{(r - 1)^2 + (\alpha - 1)^2 + (\beta - 1)^2} \quad (22)$$

336
$$NSE = 1 - \frac{\sum_{t=1}^n (Q_0 - Q_m)^2}{\sum_{t=1}^n (Q_0 - \bar{Q}_0)^2} \quad (23)$$

337
$$RMSE = \sqrt{\frac{1}{N} \sum_{i=1}^n (Q_0 - Q_m)^2} \quad (24)$$

338
$$R = \frac{\sum_{t=1}^n (Q_0 - \bar{Q}_0)(Q_m - \bar{Q}_m)}{\sqrt{\sum_{t=1}^n (Q_0 - \bar{Q}_0)^2} \sqrt{\sum_{t=1}^n (Q_m - \bar{Q}_m)^2}} \quad (25)$$

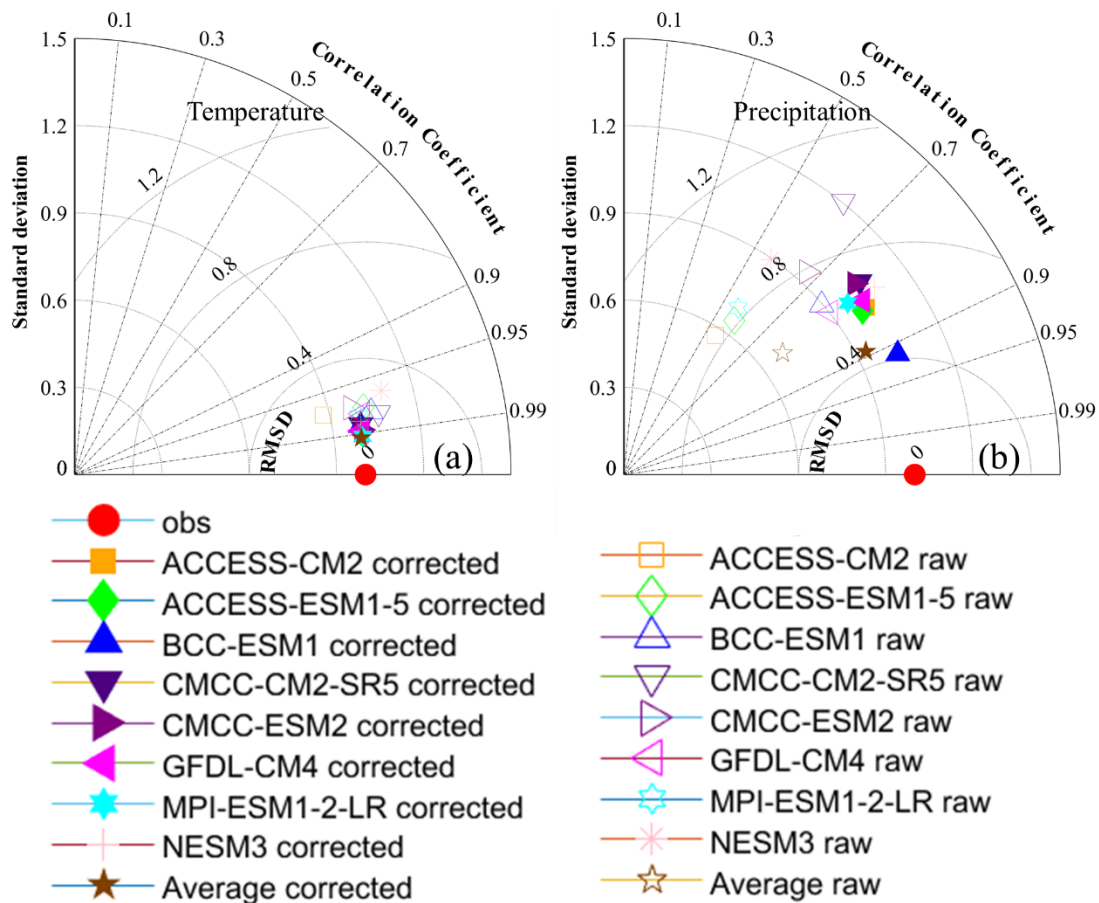
339 where, r is linear correction coefficient between simulation and observation, α is
340 the ratio of the stand deviation of simulated variables and observed variables, β is the
341 ratio of the average value of simulated and observed variables, Q_0 is the observation
342 runoff, $\overline{Q_0}$ is the average observed runoff and Q_m is the simulation runoff.

343 **4. Results**

344 **4.1 Performance of bias correction and runoff depth simulation**

345 **4.1.1 Bias correction performance**

346 The accuracy of climate projection varied with the multiple bias correction method
347 (Fig. 4). The distance between the observation and the projection is inversely
348 proportional to the accuracy. Before the bias correction, the distance is relatively far
349 especially for precipitation indicating that there is a large error between observations
350 and GCMs projection. After the bias correction, the distance diminishes, indicating that
351 the bias correction improves the accuracy, particularly for precipitation.



352

353

Figure 4. Taylor diagram of monthly temperature and precipitation simulation. The

354

hollow points are the uncorrected projection, the solid point are the corrected projection

355

and the solid red circle is the reference values (observation).

356

4.1.2 Performance of cryospheric elements and runoff simulation

357

We assessed the performance of the FLEX-Cryo model for glacier mass balance

358

change, freeze/thaw depth and runoff simulation based on historical observations.

359

Throughout the model demonstrated strong capabilities across all evaluated aspects.

360

For the glacier mass balance change, the model showed good accuracy throughout the

361

entire assessment period, the. Monthly simulations yielded a KGE is-value of 0.45,

362

NSE of 0.83, NSE is the correlation coefficient R of 0.95 and RMSE of 130.13

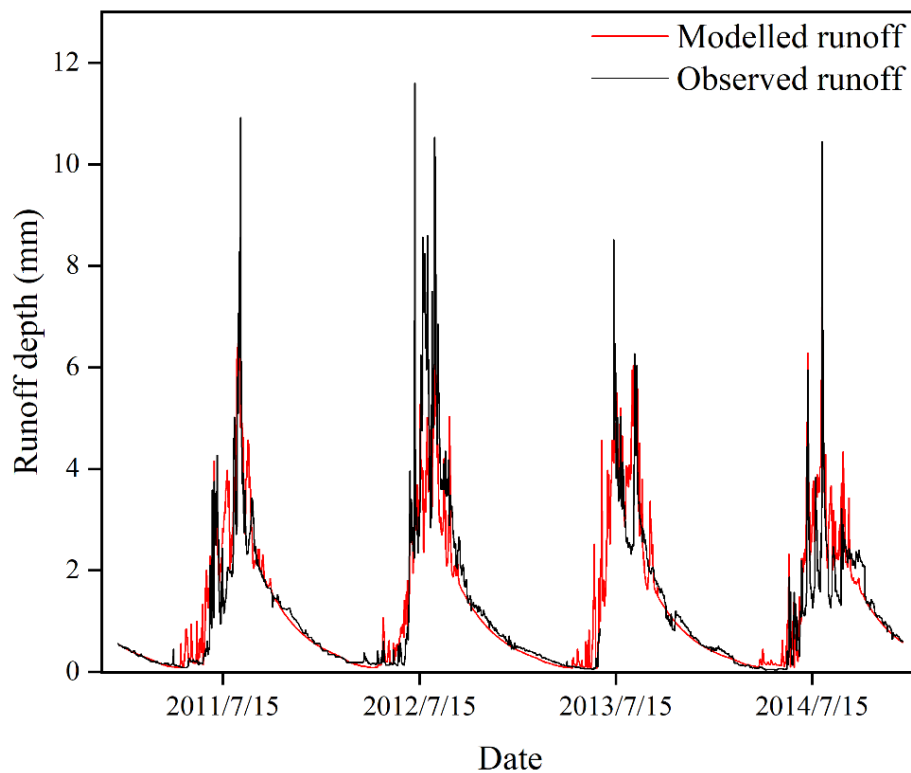
363

mm/month (Figure 5a). Regarding the free/thaw dynamics, the model accurately

364

captured both timing and duration. The simulated freeze onset consistently aligned with

365 observations, typically occurring in late October and early November. Moreover, the
366 simulated freeze-thaw cycle duration closely matched observations, with both spanning
367 approximately 217 days and varying by no more than 15 days. Notably, the model
368 exhibited exceptional accuracy in predicting maximum freezing depth, with a mere 2
369 mm error recorded in April 2013 (Figure 5b). For the runoff simulation, the model
370 showed very good performance over the assessment period, with a KGE value of 0.83,
371 NSE of 0.73, R isof 0.74, and RMSE isof 0.77 mm/day. (Figure 5c). These results
372 indicatedemonstrated that the FLEX-Cryo model can effectively reproduce
373 hydrographs effectivelyand capture changes in the cryospheric elements. The good
374 model performance in terms of various metrics demonstrates the robustness of the
375 FLEX-Cryo model, ensuring accurate estimation of providing confidence in its ability
376 to accurately estimate future hydrological changes (Fig. 5).



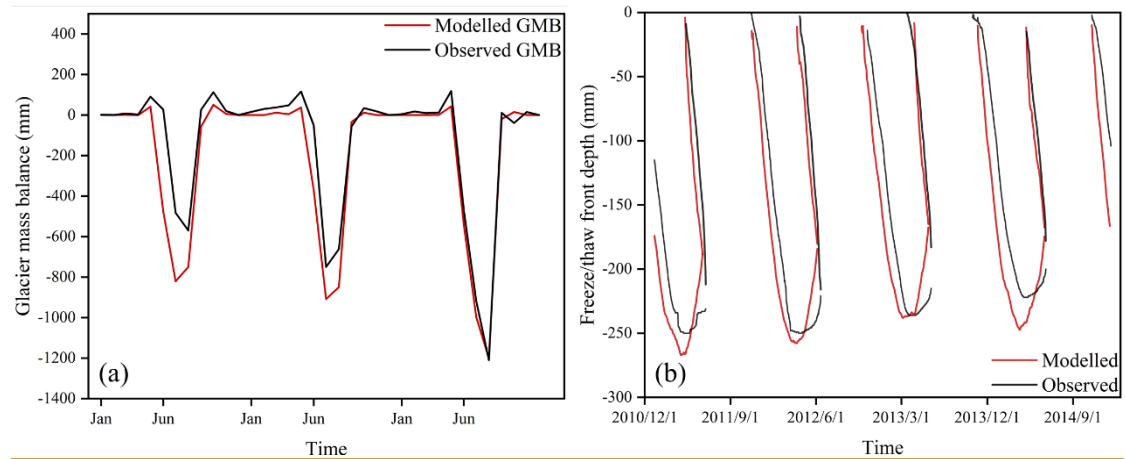
377

378

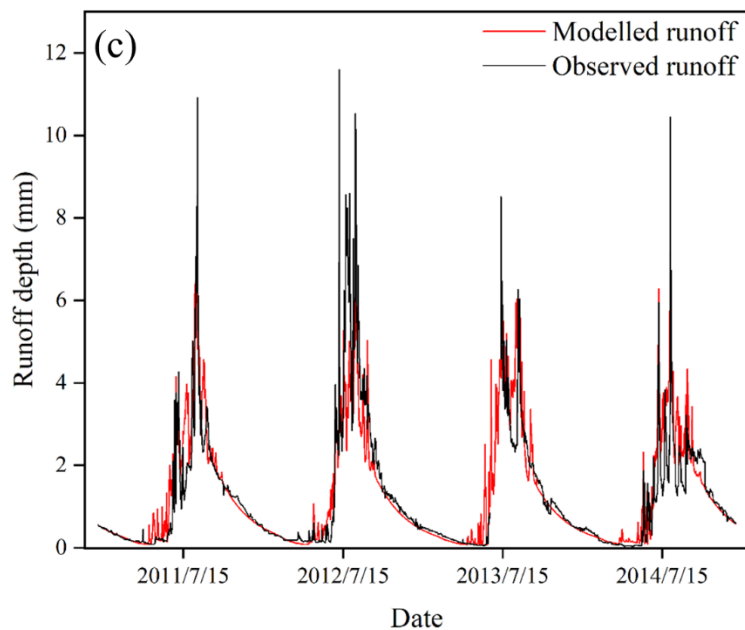
Figure.5 Simulation results of the FLEX-Cryo model and the comparisons with

379

observation from 2011 to 2014.



380



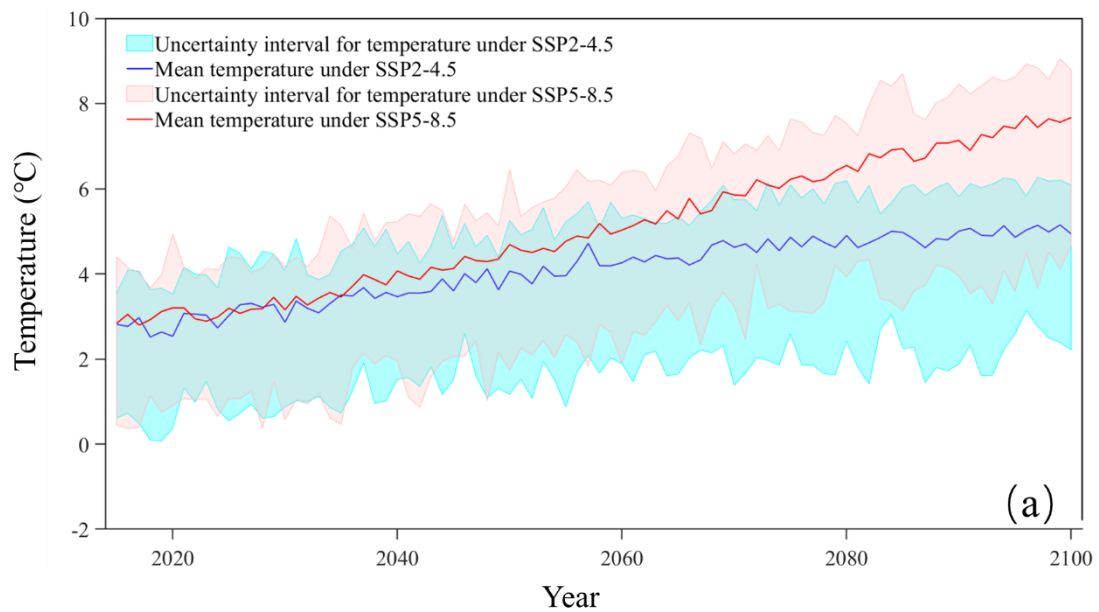
381

382 Figure.5 (a) Comparison of the modelled and observed glacier mass balance (GMB) of
 383 Glacier 1 from Jan. 2011 to Dec. 2014. (b) comparison of the simulated freeze/thaw
 384 depth by Stefan equation and observation. (c) comparison of simulated runoff by the
 385 FLEX-Cryo model and observations from 2011 to 2014.

386 4.2 Future climate change

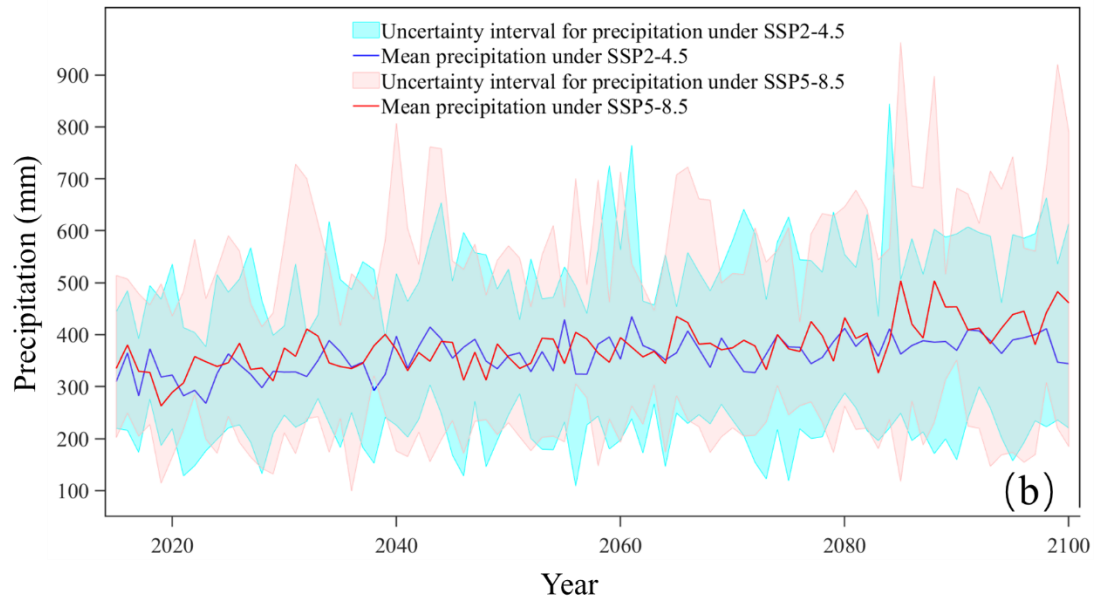
387 Figure 6 shows the prediction of future climate in 2015-2100 under the SSP2-4.5
 388 and SSP5-8.5 based on the average values of eight climate models (adjusted for bias).
 389 According to the SSP2-4.5, the temperature will increase by 2.07°C relatively steadily

390 by 2100. Under the SSP5-8.5, temperatures are projected to continue to rise by 5.04°C
391 over the course of the century. Precipitation changes are more variable than temperature,
392 especially after the eighties of the 21st century under the SSP5-8.5. Overall, the
393 precipitation under the SSP2-4.5 increased by 14.25 %, and the precipitation increased
394 by 33.50 % under the SSP5-8.5. Before the 2080s, the increase in precipitation was
395 almost the same under different scenarios, about 8.9 mm 10 years⁻¹ and 8.5 mm 10
396 years⁻¹, respectively. Although there are some uncertainties associated with temperature
397 and precipitation, the increasing trend of temperature and precipitation are still
398 distinguished, especially for the SSP5-8.5.



399

400



401

402 Figure 6. (a) the annual average temperature and (b) annual precipitation mean of
 403 bias adjusted multi-Global Climate Model from 2015-2100. The blue and red areas
 404 indicate the uncertainty caused by 8 climate change models of SSP2-4.5 and SSP 5-8.5
 405 scenarios.

406 **4.3 The change of cryosphere in the future**

407 **4.3.1 Predicting glacier retreat**

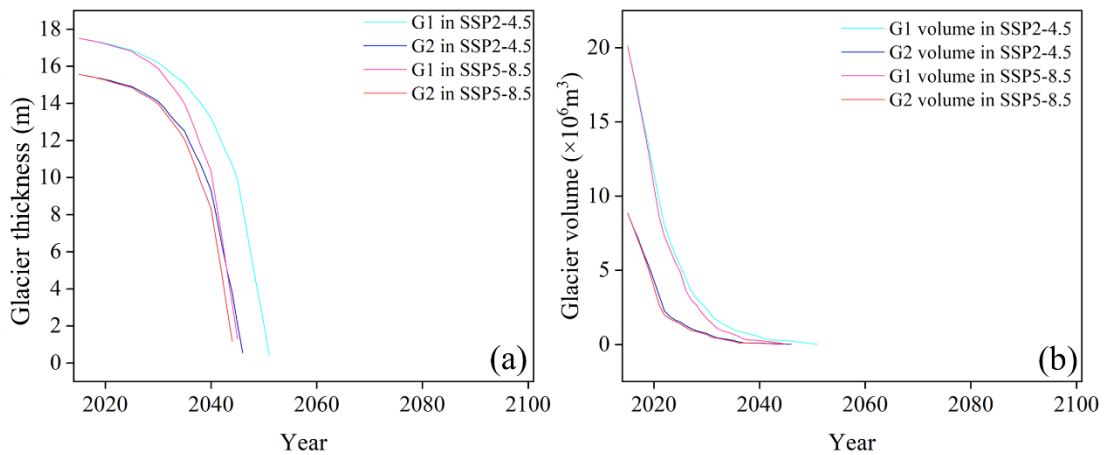
408 Figure 7 shows changes in glacier thickness at the highest elevation band and
 409 volume for the Glacier 1 and the Glacier 2 under two SSPs from years 2015–2100.
 410 Starting from the 2020s, the glacier volume showed a rapid decline, and after the 2030s,
 411 the glacier entered a phase of rapid thinning. Around 2040, the glacier degradation
 412 reached a stabilization period, during which glaciers were only present in the highest
 413 elevation band. According to the SSP2-4.5 scenario, Glacier1 and Glacier2 are
 414 projected to completely melt and disappear by 2051 and 2046, respectively. Under the
 415 SSP5-8.5 scenario, the complete melt-out time is slightly earlier, occurring in 2045 and
 416 2044 for Glacier1 and Glacier2, respectively. After the glaciers completely melt ablated

417 glacier area will transform into alpine desert.

418 Taking the glacier changes in 2025, 2035, and 2045 as examples, under the SSP2-
419 4.5 scenario, the area of Glacier1 is projected to decrease to $5.49 \times 10^5 \text{ m}^2$, $1.52 \times 10^5 \text{ m}^2$,
420 and $0.26 \times 10^5 \text{ m}^2$, with corresponding volume reductions to $5.27 \times 10^6 \text{ m}^3$, $1.03 \times 10^6 \text{ m}^3$,
421 and $0.26 \times 10^6 \text{ m}^3$, respectively (Fig. 9). Comparatively, the retreat trend is more
422 pronounced under the SSP5-8.5 scenario. The area of Glacier1 is projected to be
423 $4.00 \times 10^5 \text{ m}^2$, $0.81 \times 10^5 \text{ m}^2$, and $0.26 \times 10^5 \text{ m}^2$, with volumes of $4.86 \times 10^6 \text{ m}^3$, 0.71×10^6
424 m^3 , and $0.03 \times 10^6 \text{ m}^3$, respectively. The degradation of Glacier2 follows a similar
425 pattern to that of Glacier1, except that Glacier2 experiences less ice loss. According to
426 the SSP5-8.5 scenario, Glacier2 is projected to completely melt by 2045. In 2025 and
427 2035, the area of Glacier2 is $1.67 \times 10^5 \text{ m}^2$ and $0.51 \times 10^5 \text{ m}^2$ for both scenarios,
428 respectively. These glaciers are only distributed within the elevation bands from 4625
429 m to 4727 m and from 4675 m to 4727 m.

430

431



432

433 Figure 7. The glacier thickness (a) and glacier volume (b) change from 2015 to

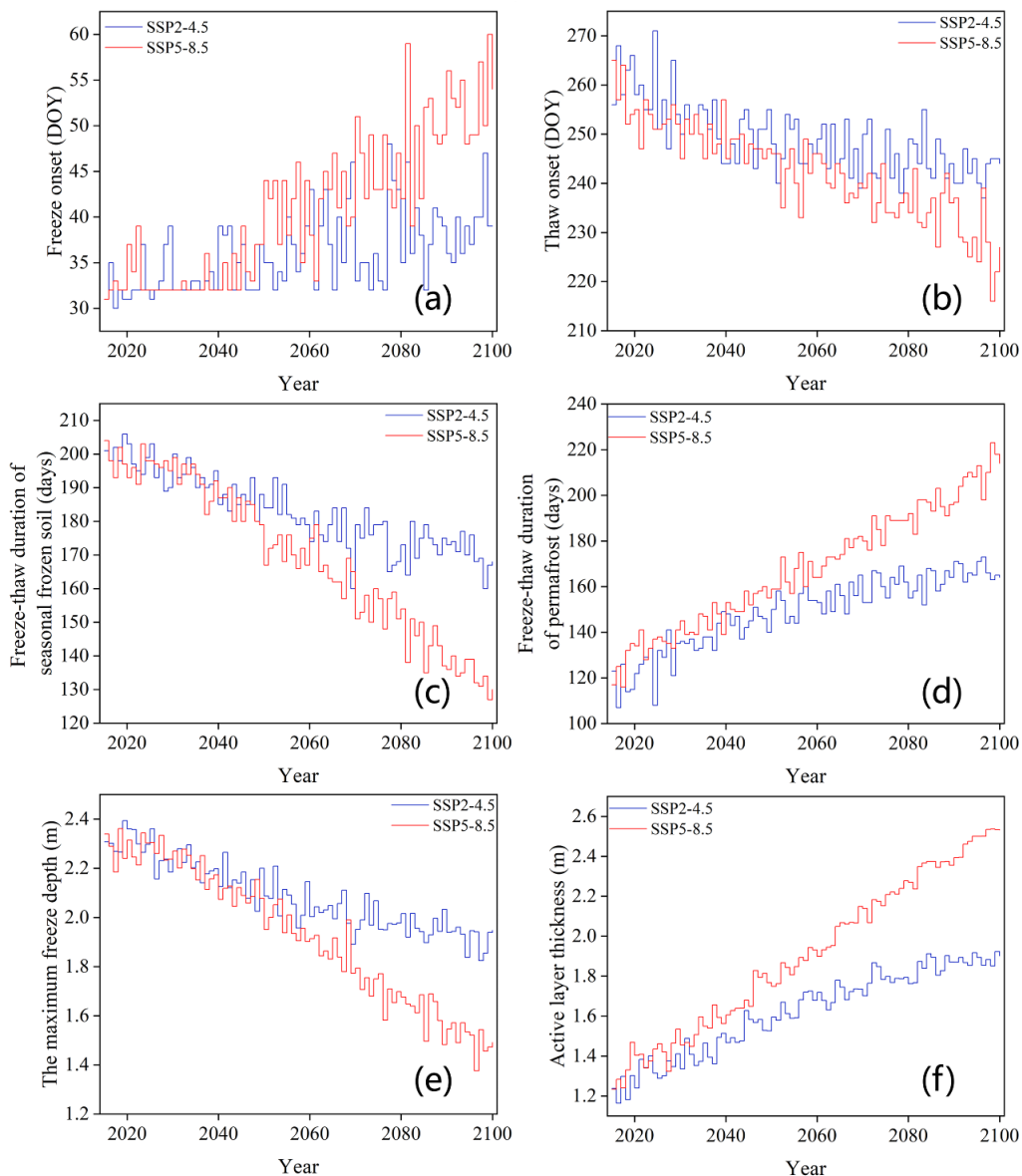
434 2100 for the Glacier1 and Glacier 2

435 4.3.2 Forecasting the degradation of frozen soil

436 The degradation of seasonally frozen soil and permafrost are projected by FLEX-
437 Cryo model. Under SSP2-4.5, by the end of 21st century, the freeze onset of seasonally
438 frozen soil will be delayed by 10 days and the freeze-thaw cycle duration will shorten
439 approximately 1 month. The maximum freeze depth of seasonally frozen soil is
440 expected to decrease by 5.17 cm per decade. The thaw onset of permafrost will be
441 advanced by 19 days and the freeze-thaw cycle duration would increase nearly 50 days.
442 The active layer thickness will rise by approximately 8.24 cm per decade. Meanwhile,
443 the degradation trend of permafrost is more severe under the SSP5-8.5 scenario. Under
444 SSP2-4.5, the freeze onset of seasonally frozen soil will be shortened by 22 days and
445 the freeze-thaw cycle duration will reduce by over 2 months. The thaw onset of
446 permafrost will occur approximately 1 month earlier, and the freeze-thaw cycle duration
447 of permafrost will increase by nearly 3 months. Compared with the SSP2-4.5, the
448 decreasing trend of the maximum freeze depth and the increasing trend of the active
449 layer thickness are approximately twice as pronounced under the SSP5-8.5. By 2100
450 Seasonally frozen soil will begin to freeze around mid-November and late November,
451 while permafrost will start to thaw in mid-May and early June by the year 2100 under
452 two SSPs.

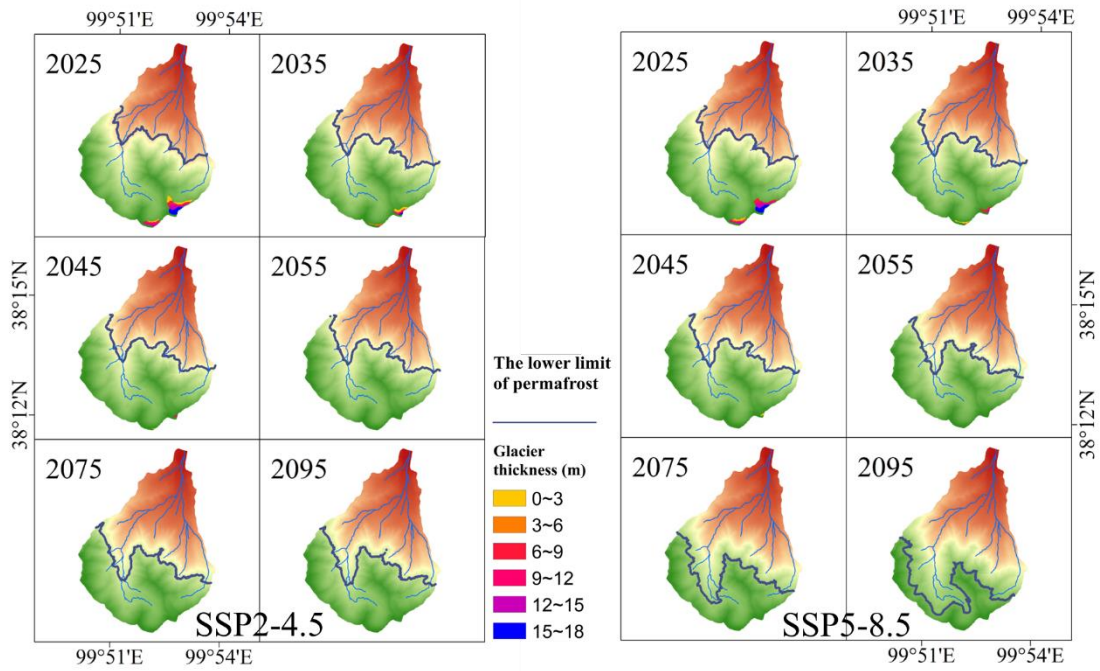
453 Under the SSP2-4.5 and SSP5-8.5, the lower limit of permafrost gradually expands
454 along the altitudinal gradient, with rates of 4.30 m per year and 8.75 m per year,
455 respectively (Fig. 9). In the SSP2-4.5, the lower limit of permafrost is projected to reach
456 altitudes of 3685 m, 3795 m, 3835 m, 3865 m, 3985 m, and 4015 m in the years 2025,
457 2035, 2045, 2055, 2075, and 2095, respectively. The lower limit of permafrost in 2095
458 under the SSP2-4.5 scenario is comparable to the lower limit of permafrost (3965m) in
459 2055 under the SSP5-8.5 scenario. The lower limit is projected to increase to 4355 m

460 by 2095 under the SSP5-8.5 scenario.



461

462 Figure 8. Changes in seasonally frozen soil and permafrost from 2015-2100 under
463 SSP2-4.5 and SSP5-8.5 scenarios. (a, b) Freeze and thaw onset. (c, d) Freeze-Thaw
464 duration of frozen soil and permafrost. (e, f) The maximum freezing depth and active
465 layer thickness.

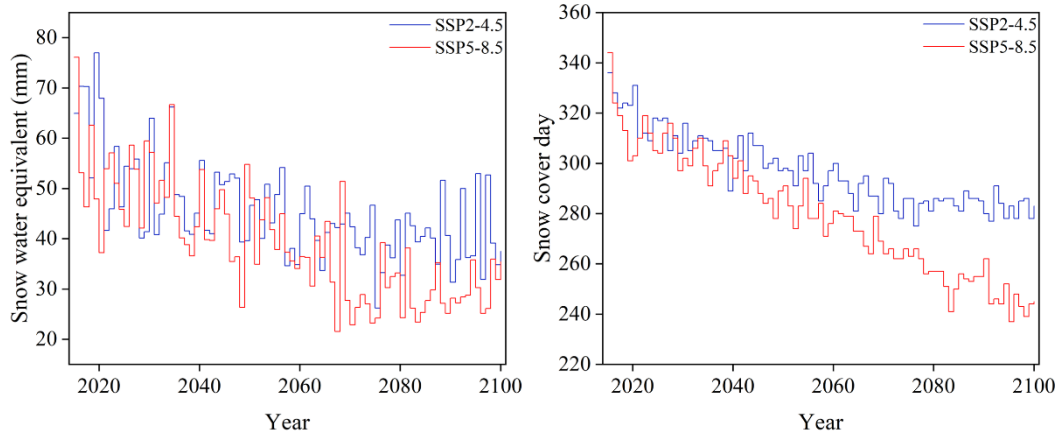


466

467 Figure 9. Changes of ice thickness and the lower limit of permafrost in 2025, 2035,
 468 2045, 2055, 2075 and 2095 under SSP2-4.5 and SSP5-8.5.

469 4.3.3 Snow change in the future

470 The duration of snow cover is projected to decrease continuously in the future (Fig.
 471 10). Under the SSP2-4.5, snow cover days are likely to be shortened by 45 days and
 472 snow water equivalent will decrease by 0.24 mm per year. Compared with SSP 2-4.5,
 473 snow cover has a more reduction under SSP5-8.5. Under SSP5-8.5, snow cover day is
 474 expected to be around 76 days and snow water equivalent will decrease by 0.35 mm
 475 per year.



476

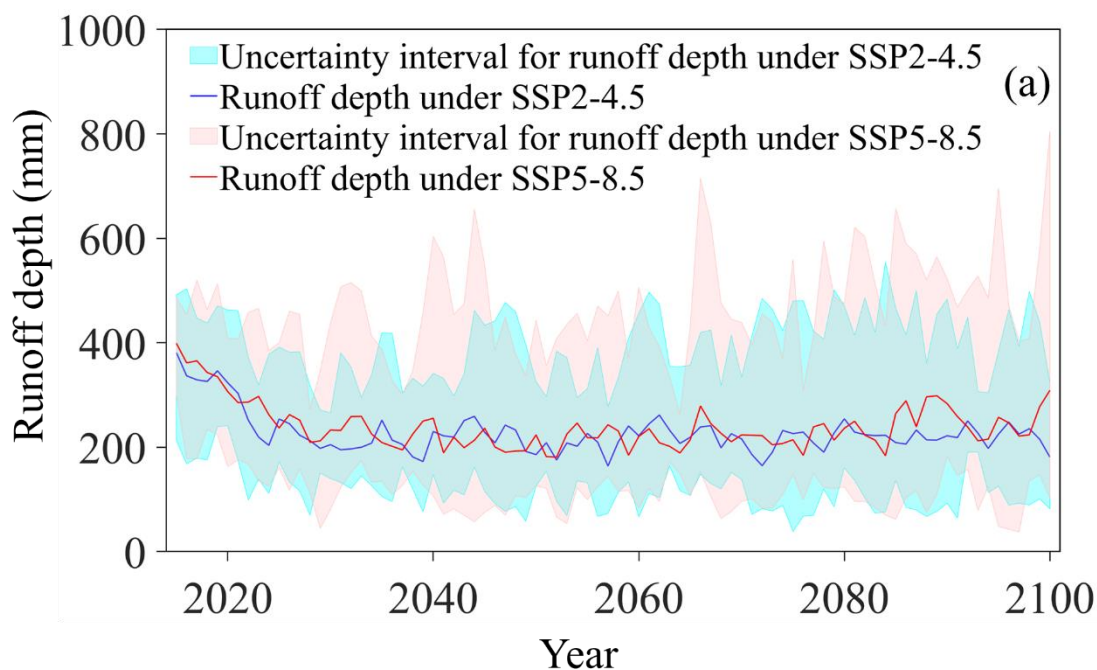
477 Figure 10. Changes of snow water equivalent and snow cover day from 2015-2100
 478 under SSP2-4.5 and SSP5-8.5.

479 4.4 Projected future runoff

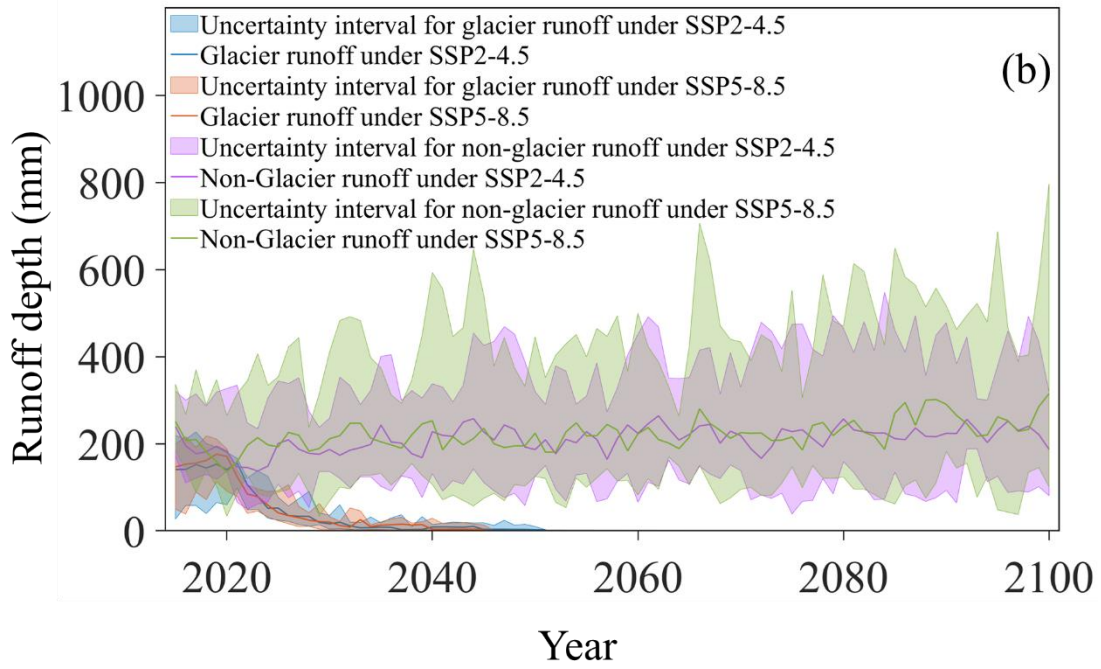
480 The runoff in the catchment were predicted by the FLEX-Cryo model under SSP2-
 481 4.5 and SSP5-8.5. The tipping point of the glacier melting has already occurred (around
 482 2020). After the turning point, glacier runoff and runoff of the total basin decreases
 483 dramatically until glacier completely melt. Then the runoff of the total basin will
 484 moderate increase. After glacier completely melt, runoff of the total basin would
 485 decrease by 15.56% and 18.05% respectively. The runoff coefficient, which represents
 486 the proportion of precipitation that becomes runoff, follows a similar pattern to the
 487 glacier runoff changes. It initially increases until the turning point of glacier melting
 488 occurs, then decreases, and eventually reaches a relatively stable state after the glaciers
 489 completely melt (Fig. 11 (c)). Before the turning point, runoff coefficient is almost equal
 490 or even greater than 1. The maximum values of the runoff coefficient occur in 2021 and
 491 2019, coinciding with the tipping points of the glacier runoff. By the end of the 21st
 492 century, the runoff coefficient is projected to be dramatically reduced to approximately
 493 0.42. These results indicate that glacier play a key role in water resource supply.

494 Two hydrological phenomena observed in permafrost mountainous catchments,

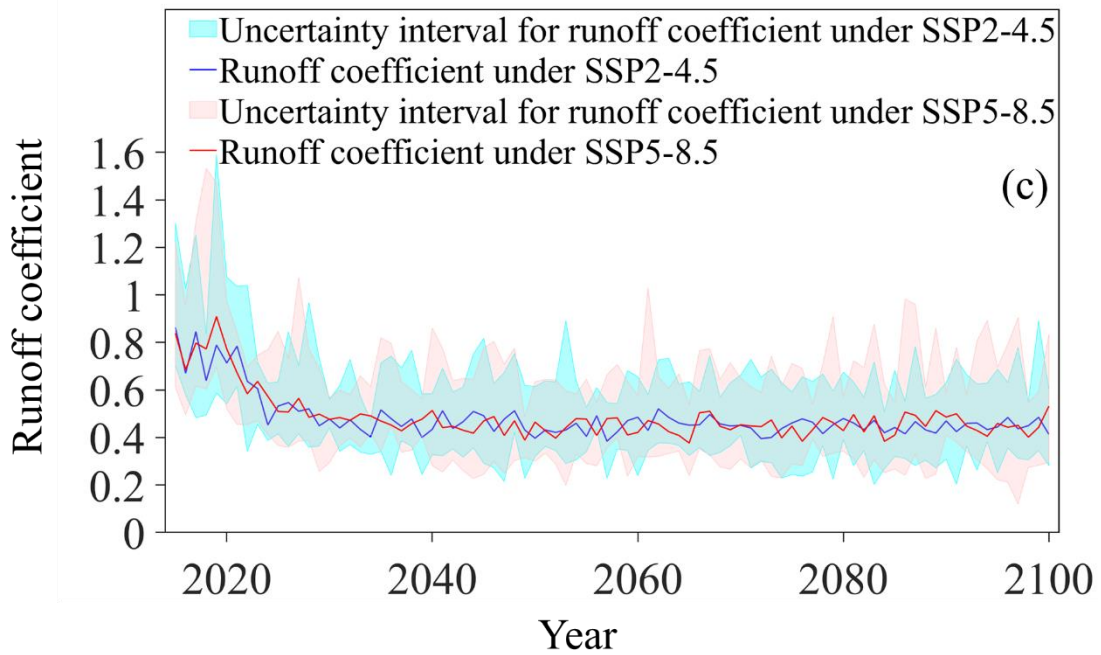
495 namely the low runoff in the early thawing season (LRET) and discontinuous baseflow
 496 recession (DBR) (Gao et al., 2022), are expected to persist in the future (Fig. 12).
 497 Meanwhile, baseflow, which represents the sustained flow of water from groundwater,
 498 shows an increasing trend. The duration of the early thawing season is projected to be
 499 further reduced. The first recession coefficient remains unchanged, while the second
 500 recession coefficient progressively increases. Under the SSP2-4.5 scenario, the second
 501 recession coefficient is equal to 74 days, which is consistent with the recession
 502 coefficient in 2060 under the SSP5-8.5 scenario. This suggests that the permafrost area
 503 undergoes less significant changes under SSP2-4.5 scenario than SSP2-8.5 scenario
 504 according to Figure 9. The baseflow gradually increases, especially in the SSP5-8.5
 505 scenario, as indicated by the runoff depth on a logarithmic scale (Fig. 12).



506

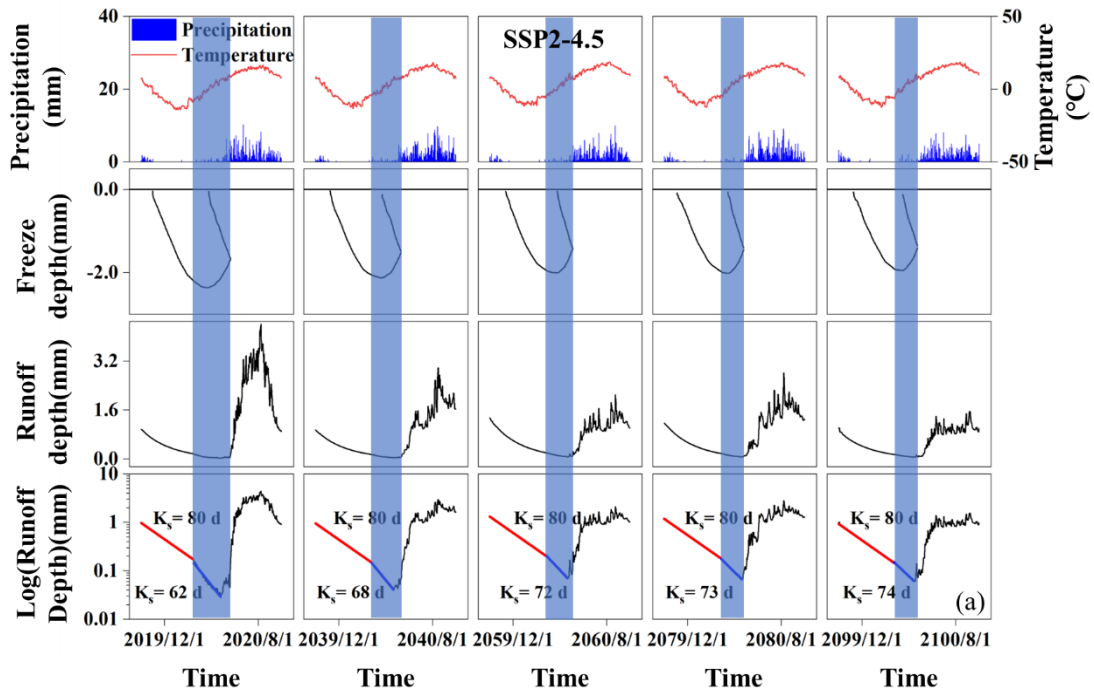


507

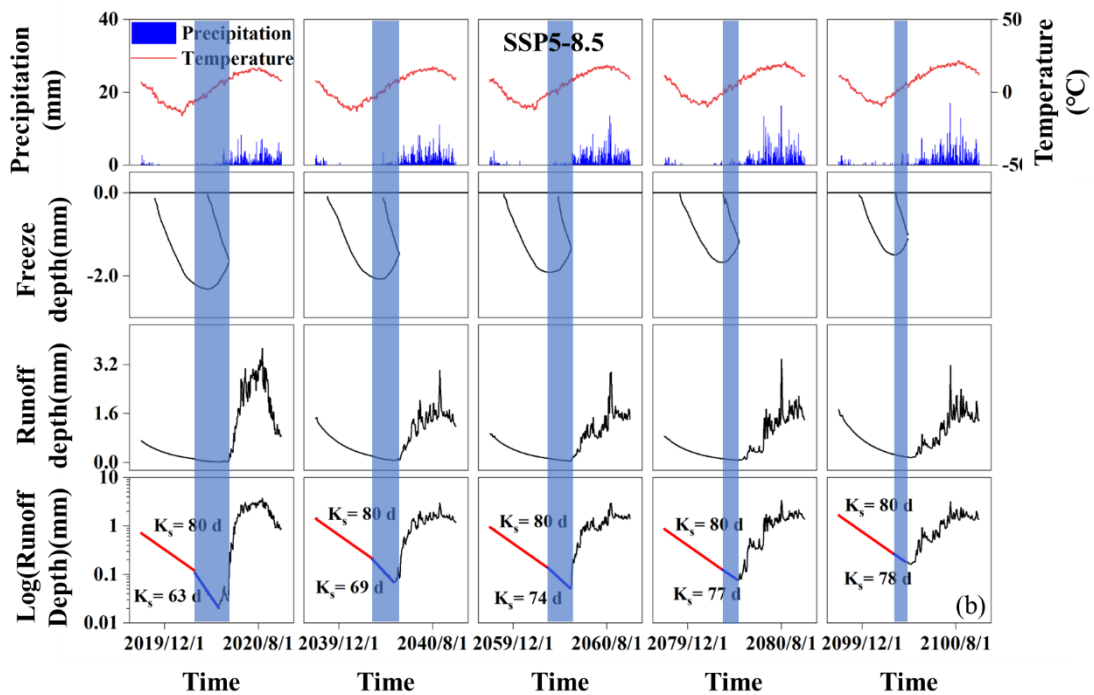


508

509 Figure 11. (a) The predicted runoff depth of the total basin. (b) Runoff in the glacier
 510 and in the non-glacier from 2015-2100. (c) Project runoff coefficient under SSP2-4.5
 511 and SSP5-8.5 scenarios.



512



513

514 Figure 12. Temperature, precipitation, runoff depth and freeze-thaw cycle in 2020,
 515 2040, 2060, 2080 and 2100 under SSP2-4.5 (a, top) and SSP5-8.5 scenarios (b, bottom).

516 **5. Discussion**

517 **5.1 The effect of the mountain cryosphere degradation on runoff**

518 Glaciers and snow are sensitive to climate change and cover play a crucial role in
519 water retention, with meltwater contributing significantly to downstream water
520 resources and the ecological environment (Stecher et al., 2023; Nan and Tian, 2024).
521 The turning point of glacier runoff represents a critical tipping point that signifies not
522 only the rapid thinning of glaciers but also the irreversible stage of water resources in
523 the basin (Brovkin et al., 2021). After the turning point the glacier thickness and glacier
524 volume rapidly decrease (Fig. 7). But the glacier thickness showed in this paper is the
525 change at the highest elevation band, which means the turning point would lag in this
526 band for change of glacier thickness. In the Hulu catchment, the proportion of glacier
527 runoff reached 51% to 55% between 2019 and 2021, indicating that it is in the turning
528 point period (Fig. 11). Subsequently, the contribution of glacier runoff gradually
529 decreases until complete melting occurs. Temperature is the primary factor influencing
530 glacier runoff, while precipitation and temperature together determine the proportion
531 of glacier runoff in relation to total runoff. Although the highest contribution of glacier
532 runoff and the tipping point of glacier runoff may not align precisely, after the tipping
533 point, the capacity of glacier runoff to contribute to overall runoff continuously
534 diminishes. From 2015 to 2021, there has been a decreasing trend in precipitation,
535 leading to a corresponding decline in non-glacier runoff (Fig. 6 and Fig. 11). Thus,
536 while glacier runoff has increased, the total runoff has decreased. However, between
537 2032 and 2038, even though rainfall continues to decline, the contribution of glacier
538 runoff to overall runoff becomes negligible due to the limited volume of ice remaining
539 (glacier volume $< 1 \times 10^6 \text{ m}^3$), resulting in minimal glacier melting runoff (Fig. 7 and
540 Fig. 11). On the other hand, once the glaciers have completely melted, the total runoff
541 in the Hulu catchment is reduced by 16% to 18%, and the runoff coefficient is halved

542 (Fig. 9 and Fig. 10). This highlights the critical role of glaciers as solid freshwater
543 reservoirs in regulating water sources and mitigating droughts (McCarthy et al., 2022).

544 The freeze-thaw cycle has a significant impact on runoff yield and hydrological
545 response routines in the Hulu catchment (Sun et al., 2022; Wang et al., 2020).

546 Precipitation in the Hulu catchment is primarily concentrated in the summer when soil
547 moisture is high and even close to saturation, making saturation excess flow the main

548 mechanism for runoff generation (Li et al., 2016). During the freeze-thaw cycle, the
549 weak permeability of frozen soil affects both surface runoff and infiltration. Soil runoff

550 primarily occurs through underground in hillslope and surface water flow in riparian
551 area, resulting in a faster response to rainfall and snowmelt and contributing to a higher

552 runoff coefficient (Hu et al., 2022; Jones et al., 2023). However, it is important to note
553 that shallow frozen soil does not completely block the interaction between deeper soil

554 layers and the surface. Frost heave in the soil creates large pores, allowing snowmelt
555 water and precipitation to bypass the matrix layer and reach the deeper soils (Jiang et

556 al., 2021; Zhang et al., 2023). This phenomenon is considered one of the significant
557 reasons for low runoff in the early thawing season (Mohammed et al., 2021). Low

558 runoff is observed between the frozen season and complete thawing season (Fig. 12).
559 The duration of freeze-thaw cycles in seasonally frozen soils is shortening, and freeze

560 onset is being delayed due to the warming climate, resulting in a decreasing duration of
561 low runoff. However, the temperature during the freezing season remains lower than

562 the initial frost heave temperature of the soil, and there is still a deficit of soil water in
563 the early thaw, indicating that the prevalence of low runoff will persist in the future

564 (Teng et al., 2022; Wen et al., 2024).

565 The freezing state has a significant impact on the recession process of baseflow,

566 and permafrost plays a crucial role in discontinuous baseflow (Cooper et al., 2023; J.
567 Wang et al., 2022). During the freezing season, baseflow follows a linear recession
568 process ($K_s = 80$ days), with contributions from both permafrost and seasonally frozen
569 soil regions (Fig. 12). In the frozen season, the groundwater under the supra-permafrost
570 layer becomes inactive, and baseflow is solely derived from the seasonally frozen soil
571 regions, causing a discontinuous recession. With climate warming, the lower limit of
572 permafrost gradually moves upward along the elevation, resulting in the shrinking of
573 the permafrost region. This suggests that in the future, an increased proportion of
574 baseflow will originate from the expanding area of seasonally frozen soil, leading to a
575 gradual decrease in the influence of permafrost on baseflow. Consequently, the
576 discontinuous recession of baseflow will gradually transition into a linear recession.
577 Furthermore, an increase in the thickness of the active layer enhances the soil water
578 storage capacity, contributing to a gradual rise in baseflow (Yao et al., 2021).

579 **5.2 Comparison with other studies**

580 The cryosphere, including glaciers (ice sheets), seasonal snow cover, frozen soil,
581 and permafrost, plays a vital role in storing approximately 75% of the world's
582 freshwater resources (Qin et al., 2021). Although there are some differences in the the
583 driving data and models, the trends of the cryospheric elements and runoff changes are
584 still comparable and consistent. In this study, the small glaciers are projected to
585 completely melt in the Mid-21st century, which is also reported in the other area
586 (Mukhopadhyay and Khan, 2015; Baraer et al., 2012; Schwank et al., 2014). The
587 projected maximum freeze depth of seasonally frozen soil calculated in this research is
588 5.2 cm per decade, similar to the 5.4 cm per decade predicted by Wang et al. (2018). Ni
589 et al. (2021) showed that Qinghai-Tibet Plateau permafrost is at risk of disappearance

590 based on statistical and machine learning (ML) modeling approaches. This shift in
591 regions with permafrost impacts hydrological connectivity, fostering improved
592 hydrothermal conditions that enhance vegetation growth (Han and Menzel, 2022; Jin et
593 al., 2022). Few studies have focused on the change in the snow cover days and snow
594 water equivalent in the Heihe river basin in the future, but many researches have
595 indicated that the snow-free period increases and the snow water equivalent decreases
596 due to climatic warming in Tibet Plateau (Zhang and Ma, 2018). The reduction of the
597 snow cover period may result in an earlier peak in spring snowmelt floods, thereby
598 increasing the risk of flooding (Chai et al., 2022). Simultaneously, the decrease in snow
599 water equivalent may impact plant water supply, placing pressure on ecosystems (Guan
600 et al., 2022). Although cryospheric elements have a trend of degradation in different
601 regions, the impact on runoff may differ. However, on a longer time scale, the
602 degradation of the cryosphere will lead to a decrease in runoff (Xu et al., 2024). This
603 study confirmed that runoff from cryospheric melting is one of the main factors
604 controlling runoff, and degradation of the cryosphere may exacerbate the risk of future
605 droughts.

606 **5.3 Uncertainty and limitations**

607 Uncertainty in this study comes from the GCMs, the downscaling and bias
608 correction methods, and the structure and parameters of the FLEX-Cryo model. The
609 temperature and precipitation projections from different GCMs at the basin scale
610 introduce uncertainty. Moreover, four bias correction methods were used to correct the
611 GCMs based on the observation, which may ensure consistent relative trends but not
612 improve the accuracy of precipitation and temperature frequency distribution and
613 seasonal variations. This may cause some uncertainty in the simulation results (Jia et

614 al., 2023).

615 In this research, the time-variant albedo information and the aspect are worthwhile
616 to be taken into account for improving glacier melting simulations, which require
617 further observation and quantitative studies (Arnold et al., 2006; Feng et al., 2024). The
618 change in elements is sensitive to energy. The snow cover and the effect of topographic
619 shading may also have an effect on the degradation and thus hydrologic response, which
620 warrants further investigation (Zhang, 2005). On a long time scale, the degradation of
621 frozen soil and glacier may result in thaw lake generation and other landscapes changes,
622 which may effect on the runoff yield and baseflow recession (Serban et al., 2021).

623 **6.Conclusions**

624 In this study, we employed the FLEX-Cryo model and data from eight Global
625 Climate Models (GCMs) under the SSP2-4.5 and SSP5-8.5 scenarios to predict the
626 potential impacts of climate change on the mountain cryosphere and hydrology. Results
627 from the projected change of mountain cryosphere elements, glacier, snow and frozen
628 soil are expected to undergo degradation. The glacier will completely melt by the
629 middle of the 21st century. Snow cover day will decrease by 45 and 76 days, and snow
630 water equivalent will decrease by 0.24mm/yr and 0.35mm/yr. The thaw onset is
631 expected to advance 19 days and 32 days. The active layer thickness will increase by
632 8.24cm/10yr.

633 The degradation of the mountain cryosphere has significant implications for water
634 resources. The tipping point of glacier runoff is projected to occur in the 2020s. Once
635 the glaciers have completely melted, the runoff is projected to decrease by
636 approximately 16% and 18% under the SSP2-4.5 and SSP5-8.5 scenarios, respectively.
637 Importantly, the duration of low runoff will shorten, baseflow will increase and the

638 discontinue recession of baseflow will gradually transform to a more linear pattern.

639 This study provides insights into the potential impacts of climate change on the
640 mountain cryosphere and hydrology. The projected changes in glacier retreat, snow
641 cover, and frozen soil dynamics highlight the urgent need for proactive water resource
642 management strategies in the face of a changing climate. Further modelling research
643 and monitoring efforts are necessary to refine these projections and guide effective
644 adaptation measures to sustainably manage water resources in mountainous regions.

645

646 **Competing interests**

647 At least one of the (co-)authors is a member of the editorial board of Hydrology and
648 Earth System Sciences.

649

650 **Acknowledgements**

651 This research has been supported by the National Natural Science Foundation of China
652 (grant no. 42071081 and 42122002). Zheng Duan acknowledges the support from the
653 Crafoord Foundation (No. [2021055220240857](#)).

654

655 **References**

656 Abdelhamed, M. S., Elshamy, M. E., Wheeler, H. S., and Razavi, S.: Hydrologic-
657 land surface modelling of the Canadian sporadic-discontinuous permafrost:
658 Initialization and uncertainty propagation, *Hydrol. Process.*, 36,
659 <https://doi.org/10.1002/hyp.14509>, 2022.

660 Adler, C., Huggel, C., Orlove, B., and Nolin, A.: Climate change in the mountain
661 cryosphere: impacts and responses, *Reg Environ Change*, 19, 1225–1228,

662 <https://doi.org/10.1007/s10113-019-01507-6>, 2019.

663 Andrianaki, M., Shrestha, J., Kobierska, F., Nikolaidis, N. P., and Bernasconi, S.
664 M.: Assessment of SWAT spatial and temporal transferability for a high-altitude
665 glacierized catchment, *Hydrol. Earth Syst. Sci.*, 23, 3219–3232,
666 <https://doi.org/10.5194/hess-23-3219-2019>, 2019.

667 Arendt, A., Krakauer, N., Kumar, S. V., Rounce, D. R., and Rupper, S.: Editorial:
668 Collaborative Research to Address Changes in the Climate, Hydrology and Cryosphere
669 of High Mountain Asia, *Front. Earth Sci.*, 8, 605336,
670 <https://doi.org/10.3389/feart.2020.605336>, 2020.

671 Arnold, N. S., Rees, W. G., Hodson, A. J., and Kohler, J.: Topographic controls on
672 the surface energy balance of a high Arctic valley glacier, *J. Geophys. Res.*, 111,
673 2005JF000426, <https://doi.org/10.1029/2005JF000426>, 2006.

674 Aubry-Wake, C. and Pomeroy, J. W.: Predicting Hydrological Change in an Alpine
675 Glacierized Basin and Its Sensitivity to Landscape Evolution and Meteorological
676 Forcings, *Water Resour. Res.*, 59, <https://doi.org/10.1029/2022WR033363>, 2023.

677 Baraer, M., Mark, B. G., McKenzie, J. M., Condom, T., Bury, J., Huh, K.-I.,
678 Portocarrero, C., Gómez, J., and Rathay, S.: Glacier recession and water resources in
679 Peru's Cordillera Blanca, *J. Glaciol.*, 58, 134–150,
680 <https://doi.org/10.3189/2012JoG11J186>, 2012.

681 Blöschl, G., Bierkens, M. F. P., Chambel, A., Cudennec, C., Destouni, G., Fiori,
682 A., Kirchner, J. W., McDonnell, J. J., Savenije, H. H. G., Sivapalan, M., Stump, C.,
683 Toth, E., Volpi, E., Carr, G., Lupton, C., Salinas, J., Széles, B., Viglione, A., Aksoy, H.,
684 Allen, S. T., Amin, A., Andréassian, V., Arheimer, B., Aryal, S. K., Baker, V., Bardsley,
685 E., Barendrecht, M. H., Bartosova, A., Batelaan, O., Berghuijs, W. R., Beven, K., Blume,

686 T., Bogaard, T., Borges De Amorim, P., Böttcher, M. E., Boulet, G., Breinl, K., Brilly,
687 M., Brocca, L., Buytaert, W., Castellarin, A., Castelletti, A., Chen, X., Chen, Y., Chen,
688 Y., Chiffard, P., Claps, P., Clark, M. P., Collins, A. L., Croke, B., Dathe, A., David, P.
689 C., De Barros, F. P. J., De Rooij, G., Di Baldassarre, G., Driscoll, J. M., Duethmann, D.,
690 Dwivedi, R., Eris, E., Farmer, W. H., Feiccabrino, J., Ferguson, G., Ferrari, E., Ferraris,
691 S., Fersch, B., Finger, D., Foglia, L., Fowler, K., Gartsman, B., Gascoin, S., Gaume, E.,
692 Gelfan, A., Geris, J., Gharari, S., Gleeson, T., Glendell, M., Gonzalez Bevacqua, A.,
693 González-Dugo, M. P., Grimaldi, S., Gupta, A. B., Guse, B., Han, D., Hannah, D.,
694 Harpold, A., Haun, S., Heal, K., Helfricht, K., Herrnegger, M., Hipsey, M., Hlaváčiková,
695 H., Hohmann, C., Holko, L., Hopkinson, C., Hrachowitz, M., Illangasekare, T. H., Inam,
696 A., Innocente, C., Istanbuluoglu, E., Jarihani, B., et al.: Twenty-three unsolved
697 problems in hydrology (UPH) – a community perspective, *Hydrology. Sci. J.*, 64, 1141–
698 1158, <https://doi.org/10.1080/02626667.2019.1620507>, 2019.

699 Bolibar, J., Rabatel, A., Gouttevin, I., Zekollari, H., and Galiez, C.: Nonlinear
700 sensitivity of glacier mass balance to future climate change unveiled by deep learning,
701 *Nat. Commun.*, 13, 409, <https://doi.org/10.1038/s41467-022-28033-0>, 2022.

702 Brovkin, V., Brook, E., Williams, J. W., Bathiany, S., Lenton, T. M., Barton, M.,
703 DeConto, R. M., Donges, J. F., Ganopolski, A., McManus, J., Praetorius, S., De Vernal,
704 A., Abe-Ouchi, A., Cheng, H., Claussen, M., Crucifix, M., Gallopín, G., Iglesias, V.,
705 Kaufman, D. S., Kleinen, T., Lambert, F., Van Der Leeuw, S., Liddy, H., Loutre, M.-F.,
706 McGee, D., Rehfeld, K., Rhodes, R., Seddon, A. W. R., Trauth, M. H., Vanderveken,
707 L., and Yu, Z.: Past abrupt changes, tipping points and cascading impacts in the Earth
708 system, *Nat. Geosci.*, 14, 550–558, <https://doi.org/10.1038/s41561-021-00790-5>, 2021.

709 Chadburn, S. E., Burke, E. J., Cox, P. M., Friedlingstein, P., Hugelius, G., and

710 Westermann, S.: An observation-based constraint on permafrost loss as a function of
711 global warming, *Nature Clim. Change*, 7, 340–344,
712 <https://doi.org/10.1038/nclimate3262>, 2017.

713 Chai, C., Wang, L., Chen, D., Zhou, J., Liu, H., Zhang, J., Wang, Y., Chen, T., and
714 Liu, R.: Future snow changes and their impact on the upstream runoff in Salween,
715 *Hydrol. Earth Syst. Sci.*, 26, 4657–4683, <https://doi.org/10.5194/hess-26-4657-2022>,
716 2022.

717 Chang, Z., Qi, P., Zhang, G., Sun, Y., Tang, X., Jiang, M., Sun, J., and Li, Z.:
718 Latitudinal characteristics of frozen soil degradation and their response to climate
719 change in a high-latitude water tower, *CATENA*, 214, 106272,
720 <https://doi.org/10.1016/j.CATENA.2022.106272>, 2022.

721 Chen, R., Duan, K., Shang, W., Shi, P., Meng, Y., and Zhang, Z.: Increase in
722 seasonal precipitation over the Tibetan Plateau in the 21st century projected using
723 CMIP6 models, *Atmospheric Research*, 277, 106306,
724 <https://doi.org/10.1016/j.atmosres.2022.106306>, 2022

725 Chen, R. S., Lu, S.-H., Kang, E. S., Ji, X., Zhang, Z., Yang, Y., and Qing, W.: A
726 distributed water-heat coupled model for mountainous watershed of an inland river
727 basin of Northwest China (I) model structure and equations, *Environ. Geol.*, 53, 1299–
728 1309, <https://doi.org/10.1007/s00254-007-0738-2>, 2008.

729 Connon, R. F., Chasmer, L., Haughton, E., Helbig, M., Hopkinson, C., Sonnentag,
730 O., and Quinton, W. L.: The implications of permafrost thaw and land cover change on
731 snow water equivalent accumulation, melt and runoff in discontinuous permafrost
732 peatlands, *Hydrol. Process.*, 35, e14363, <https://doi.org/10.1002/hyp.14363>, 2021.

733 Cooper, M. G., Zhou, T., Bennett, K. E., Bolton, W. R., Coon, E. T., Fleming, S.

734 W., Rowland, J. C., and Schwenk, J.: Detecting Permafrost Active Layer Thickness
735 Change From Nonlinear Baseflow Recession, *Water Resour. Res.*, 59,
736 <https://doi.org/10.1029/2022WR033154>, 2023.

737 Cullen, N. J., Sirguey, P., Mölg, T., Kaser, G., Winkler, M., and Fitzsimons, S. J.:
738 A century of ice retreat on Kilimanjaro: the mapping reloaded, *The Cryosphere*, 7, 419–
739 431, <https://doi.org/10.5194/tc-7-419-2013>, 2013.

740 Ding, Y., Zhang, S., Zhao, L., Li, Z., and Kang, S.: Global warming weakening the
741 inherent stability of glaciers and permafrost, *Sci. Bull.*, 64, 245–253,
742 <https://doi.org/10.1016/j.scib.2018.12.028>, 2019.

743 Ding, Y., Zhang, S., and Chen, R.: Cryospheric Hydrology: Decode the Largest
744 Freshwater Reservoir on Earth, *Bulletin of the Chinese Academy of Sciences*, 35, 414–
745 424, 2020.

746 Elshamy, M. E., Princz, D., Sapriza-Azuri, G., Abdelhamed, M. S., Pietroniro, A.,
747 Wheeler, H. S., and Razavi, S.: On the configuration and initialization of a large-scale
748 hydrological land surface model to represent permafrost, *Hydrol. Earth Syst. Sci.*, 24,
749 349–379, <https://doi.org/10.5194/hess-24-349-2020>, 2020.

750 Farinotti, D., Huss, M., Fürst, J. J., Landmann, J., Machguth, H., Maussion, F., and
751 Pandit, A.: A consensus estimate for the ice thickness distribution of all glaciers on
752 Earth, *Nat. Geosci.*, 12, 168–173, <https://doi.org/10.1038/s41561-019-0300-3>, 2019.

753 Feng, S., Cook, J. M., Naegeli, K., Anesio, A. M., Benning, L. G., and Tranter, M.:
754 The Impact of Bare Ice Duration and Geo - Topographical Factors on the Darkening of
755 the Greenland Ice Sheet, *Geophysical Research Letters*, 51, e2023GL104894,
756 <https://doi.org/10.1029/2023GL104894>, 2024.

757 Fenicia, F. and McDonnell, J. J.: Modeling streamflow variability at the regional

758 scale: (1) perceptual model development through signature analysis, *J. Hydrol.*, 605,
759 127287, <https://doi.org/10.1016/j.jhydrol.2021.127287>, 2022.

760 Gao, H., Han, C., Chen, R., Feng, Z., Wang, K., Fenicia, F., and Savenije, H.:
761 Frozen soil hydrological modeling for a mountainous catchment northeast of the
762 Qinghai–Tibet Plateau, *Hydrol. Earth Syst. Sci.*, 26, 4187–4208,
763 <https://doi.org/10.5194/hess-26-4187-2022>, 2022.

764 Gao, H., Feng, Z., Zhang, T., Wang, Y., He, X., Li, H., Pan, X., Ren, Z., Chen, X.,
765 Zhang, W., and Duan, Z.: Assessing glacier retreat and its impact on water resources in
766 a headwater of Yangtze River based on CMIP6 projections, *Science of The Total*
767 *Environment*, 765, 142774, <https://doi.org/10.1016/j.scitotenv.2020.142774>, 2021.

768 Gao, T., Kang, S., Chen, R., Zhang, T., Zhang, T., Han, C., Tripathee, L., Sillanpää,
769 M., and Zhang, Y.: Riverine dissolved organic carbon and its optical properties in a
770 permafrost region of the Upper Heihe River basin in the Northern Tibetan Plateau, *Sci.*
771 *Total Environ.*, 686, 370–381, <https://doi.org/10.1016/j.scitotenv.2019.05.478>, 2019.

772 Gilg, O., Kovacs, K. M., Aars, J., Fort, J., Gauthier, G., Grémillet, D., Ims, R. A.,
773 Meltofte, H., Moreau, J., Post, E., Schmidt, N. M., Yannic, G., and Bollache, L.: Climate
774 change and the ecology and evolution of Arctic vertebrates, *Ann. Ny. Acad. Sci.*, 1249,
775 166–190, <https://doi.org/10.1111/j.1749-6632.2011.06412.x>, 2012.

776 Giovando, J. and Niemann, J. D.: Wildfire Impacts on Snowpack Phenology in a
777 Changing Climate Within the Western U.S., *Water Resour. Res.*, 58, e2021WR031569,
778 <https://doi.org/10.1029/2021WR031569>, 2022.

779 Gisnås, K., Westermann, S., Schuler, T. V., Melvold, K., and Etzelmüller, B.:
780 Small-scale variation of snow in a regional permafrost model, *The Cryosphere*, 10,
781 1201–1215, <https://doi.org/10.5194/tc-10-1201-2016>, 2016.

782 Guan, X., Guo, S., Huang, J., Shen, X., Fu, L., and Zhang, G.: Effect of seasonal
783 snow on the start of growing season of typical vegetation in Northern Hemisphere,
784 *Geography and Sustainability*, 3, 268–276,
785 <https://doi.org/10.1016/j.geosus.2022.09.001>, 2022.

786 Hamon, W.R.: Estimating potential evapotranspiration. *J. Hydraul. Div.-ASCE* 87,
787 107–120, 1961.

788 Han, L. and Menzel, L.: Hydrological variability in southern Siberia and the role
789 of permafrost degradation, *J. Hydrol.*, 604, 127203,
790 <https://doi.org/10.1016/j.jhydrol.2021.127203>, 2022.

791 He, Q., Kuang, X., Chen, J., Hao, Y., Feng, Y., Wu, P., and Zheng, C.: Glacier
792 retreat and its impact on groundwater system evolution in the Yarlung Zangbo source
793 region, Tibetan Plateau, *J. Hydrol.: Regional Studies*, 47, 101368,
794 <https://doi.org/10.1016/j.ejrh.2023.101368>, 2023.

795 He, Z., Duethmann, D., and Tian, F.: A meta-analysis based review of quantifying
796 the contributions of runoff components to streamflow in glacierized basins. *J. Hydrol.*,
797 603, 126890, <https://doi.org/10.1016/j.jhydrol.2021.126890>, 2021.

798 Hu, G., Li, X., Yang, X., Shi, F., Sun, H., and Cui, B.: Identifying Spatiotemporal
799 Patterns of Hillslope Subsurface Flow in an Alpine Critical Zone on the Qinghai -
800 Tibetan Plateau Based on Three - Year, High - Resolution Field Observations, *Water*
801 *Resour. Res.*, 58, e2022WR032098, <https://doi.org/10.1029/2022WR032098>, 2022.

802 Huss, M. and Fischer, M.: Sensitivity of Very Small Glaciers in the Swiss Alps to
803 Future Climate Change, *Front. Earth Sci.*, 4, <https://doi.org/10.3389/feart.2016.00034>,
804 2016.

805 Huss, M. and Hock, R.: Global-scale hydrological response to future glacier mass

806 loss, *Nature Clim Change*, 8, 135–140, <https://doi.org/10.1038/s41558-017-0049-x>,
807 2018.

808 Huss, M., Jouvét, G., Farinotti, D., and Bauder, A.: Future high-mountain
809 hydrology: a new parameterization of glacier retreat, *Hydrol. Earth Syst. Sci.*, 14, 815–
810 829, <https://doi.org/10.5194/hess-14-815-2010>, 2010.

811 Intergovernmental Panel On Climate Change (Ipcc): *The Ocean and Cryosphere*
812 *in a Changing Climate: Special Report of the Intergovernmental Panel on Climate*
813 *Change*, 1st ed., Cambridge University Press, <https://doi.org/10.1017/9781009157964>,
814 2022.

815 Jia, Q., Jia, H., Li, Y., and Yin, D.: Applicability of CMIP5 and CMIP6 Models in
816 China: Reproducibility of Historical Simulation and Uncertainty of Future Projection,
817 *Journal of Climate*, 36, 5809–5824, <https://doi.org/10.1175/JCLI-D-22-0375.1>, 2023.

818 Jiang, R., Li, T., Liu, D., Fu, Q., Hou, R., Li, Q., Cui, S., and Li, M.: Soil infiltration
819 characteristics and pore distribution under freezing–thawing conditions, *The*
820 *Cryosphere*, 15, 2133–2146, <https://doi.org/10.5194/tc-15-2133-2021>, 2021.

821 Jin, X., Jin, H., Luo, D., Sheng, Y., Wu, Q., Wu, J., Wang, W., Huang, S., Li, X.,
822 Liang, S., Wang, Q., He, R., Serban, R. D., Ma, Q., Gao, S., and Li, Y.: Impacts of
823 Permafrost Degradation on Hydrology and Vegetation in the Source Area of the Yellow
824 River on Northeastern Qinghai-Tibet Plateau, Southwest China, *Front. Earth Sci.*, 10,
825 845824, <https://doi.org/10.3389/feart.2022.845824>, 2022.

826 Jones, M. W., Sebestyen, S. D., Dymond, S. F., Ng, G. H. C., and Feng, X.: Soil
827 frost controls streamflow generation processes in headwater catchments, *J. Hydrol.*, 617,
828 <https://doi.org/10.1016/j.jhydrol.2022.128801>, 2023.

829 Kaplan Pastíriková, L., Hrbáček, F., Uxa, T., and Láska, K.: Permafrost table

830 temperature and active layer thickness variability on James Ross Island, Antarctic
831 Peninsula, in 2004–2021, *Sci. Total Environ.*, 869, 161690,
832 <https://doi.org/10.1016/j.scitotenv.2023.161690>, 2023.

833 Li, L., Xu, Z., Zuo, D., and Zhao, J.: A grid-based integrated surface–groundwater
834 model (GISMOD), *J. Water Clim. Change*, 7, 296–320,
835 <https://doi.org/10.2166/wcc.2015.006>, 2016.

836 Li, X., Jin, H., Sun, L., Wang, H., Huang, Y., He, R., Chang, X., Yu, S., and Zang,
837 S.: TTOP - model - based maps of permafrost distribution in Northeast China for
838 1961 - 2020, *Permafrost periglac*, 33, 425–435, <https://doi.org/10.1002/ppp.2157>,
839 2022.

840 Li, Z., Feng, Q., Chen, W., Wang, T., Cheng, Yan, G., Xiaoyan, G., Yanhui, P.,
841 Jianguo, L., Rui, G., and Bing, J.: Study on the contribution of cryosphere to runoff in
842 the cold alpine basin: A case study of Hulugou River Basin in the Qilian Mountains,
843 *Global and Planetary Change*, 122, 345–361,
844 <https://doi.org/10.1016/j.gloplacha.2014.10.001>, 2014.

845 Liu, J. and Chen, R.: Discriminating types of precipitation in Qilian Mountains,
846 Tibetan Plateau, *Journal of Hydrology: Regional Studies*, 5, 20–32,
847 <https://doi.org/10.1016/j.ejrh.2015.11.013>, 2016.

848 Liu, Z., Cuo, L., and Sun, N.: Tracking snowmelt during hydrological surface
849 processes using a distributed hydrological model in a mesoscale basin on the Tibetan
850 Plateau, *J. Hydrol.*, 616, <https://doi.org/10.1016/j.jhydrol.2022.128796>, 2023.

851 Ma, J., Li, R., Huang, Z., Wu, T., Wu, X., Zhao, L., Liu, H., Hu, G., Xiao, Y., Du,
852 Y., Yang, S., Liu, W., Jiao, Y., and Wang, S.: Evaluation and spatio-temporal analysis
853 of surface energy flux in permafrost regions over the Qinghai-Tibet Plateau and Arctic

854 using CMIP6 models, *International Journal of Digital Earth*, 15, 1947–1965,
855 <https://doi.org/10.1080/17538947.2022.2142307>, 2022.

856 Martin, L. C. P., Westermann, S., Magni, M., Brun, F., Fiddes, J., Lei, Y.,
857 Kraaijenbrink, P., Mathys, T., Langer, M., Allen, S., and Immerzeel, W. W.: Recent
858 ground thermo-hydrological changes in a southern Tibetan endorheic catchment and
859 implications for lake level changes, *Hydrol. Earth Syst. Sci.*, 27, 4409–4436,
860 <https://doi.org/10.5194/hess-27-4409-2023>, 2023

861 McCarthy, M., Meier, F., Fatichi, S., Stocker, B. D., Shaw, T. E., Miles, E.,
862 Dussailant, I., and Pellicciotti, F.: Glacier Contributions to River Discharge During the
863 Current Chilean Megadrought, *Earth's Future*, 10, e2022EF002852,
864 <https://doi.org/10.1029/2022EF002852>, 2022.

865 Michel, A., Schaefli, B., Wever, N., Zekollari, H., Lehning, M., and Huwald, H.:
866 Future water temperature of rivers in Switzerland under climate change investigated
867 with physics-based models, *Hydrol. Earth Syst. Sci.*, 26, 1063–1087,
868 <https://doi.org/10.5194/hess-26-1063-2022>, 2022.

869 Miner, K., Turetsky, M., Malina, E., Bartsch, A., Tamminen, J., McGuire, A., Fix,
870 A., Sweeney, C., Elder, C., and Miller, C.: Permafrost carbon emissions in a changing
871 Arctic, *Nature Reviews Earth & Environmental*, 3, 55–67,
872 <https://doi.org/10.1038/s43017-021-00230-3>, 2022.

873 Mohammed, A. A., Cey, E. E., Hayashi, M., and Callaghan, M., V.: Simulating
874 preferential flow and snowmelt partitioning in seasonally frozen hillslopes, *Hydrol.*
875 *Process.*, 35, <https://doi.org/10.1002/hyp.14277>, 2021.

876 Moreno, P. I., Fercovic, E. I., Soteres, R. L., Ugalde, P. I., Sagredo, E. A., and
877 Villa-Martínez, R. P.: Glacier and terrestrial ecosystem evolution in the Chilotan

878 archipelago sector of northwestern Patagonia since the Last Glacial Termination, Earth-
879 Science Reviews, 235, 104240, <https://doi.org/10.1016/j.earscirev.2022.104240>, 2022.

880 Mukhopadhyay, B. and Khan, A.: A reevaluation of the snowmelt and glacial melt
881 in river flows within Upper Indus Basin and its significance in a changing climate,
882 Journal of Hydrology, 527, 119–132, <https://doi.org/10.1016/j.jhydrol.2015.04.045>,
883 2015.

884 Nan, Y. and Tian, F.: Glaciers determine the sensitivity of hydrological processes
885 to perturbed climate in a large mountainous basin on the Tibetan Plateau, Hydrol. Earth
886 Syst. Sci., 28, 669–689, <https://doi.org/10.5194/hess-28-669-2024>, 2024.

887 Negi, V. S., Tiwari, D. C., Singh, L., Thakur, S., and Bhatt, I. D.: Review and
888 synthesis of climate change studies in the Himalayan region, Environ Dev Sustain, 24,
889 10471–10502, <https://doi.org/10.1007/s10668-021-01880-5>, 2022.

890 Ni, J., Wu, T., Zhu, X., Hu, G., Zou, D., Wu, X., Li, R., Xie, C., Qiao, Y., Pang, Q.,
891 Hao, J., and Yang, C.: Simulation of the Present and Future Projection of Permafrost on
892 the Qinghai - Tibet Plateau with Statistical and Machine Learning Models, JGR
893 Atmospheres, 126, e2020JD033402, <https://doi.org/10.1029/2020JD033402>, 2021.

894 Nury, A. H., Sharma, A., Mehrotra, R., Marshall, L., and Cordery, I.: Projected
895 Changes in the Tibetan Plateau Snowpack Resulting From Rising Global Temperatures,
896 J. Geophys. Res.-Atmos. , 127, <https://doi.org/10.1029/2021JD036201>, 2022.

897 Peng, Z., Tian, F., Wu, J., Huang, J., Hu, H., and Darnault, C. J. G.: A numerical
898 model for water and heat transport in freezing soils with nonequilibrium ice - water
899 interfaces, Water Resources Research, 52, 7366 – 7381,
900 <https://doi.org/10.1002/2016WR019116>, 2016.

901 Pomeroy, J. W., Brown, T., Fang, X., Shook, K. R., Pradhananga, D., Armstrong,

902 R., Harder, P., Marsh, C., Costa, D., Krogh, S. A., Aubry-Wake, C., Annand, H.,
903 Lawford, P., He, Z., Kompanizare, M., and Lopez Moreno, J. I.: The cold regions
904 hydrological modelling platform for hydrological diagnosis and prediction based on
905 process understanding, *J. Hydrol.*, 615, 128711,
906 <https://doi.org/10.1016/j.jhydrol.2022.128711>, 2022.

907 Pothula, S. K. and Adams, B. J.: Community assembly in the wake of glacial
908 retreat: A meta - analysis, *Glob. Chang Biol*, 28, 6973–6991,
909 <https://doi.org/10.1111/gcb.16427>, 2022.

910 Qin, D., Yao, T., Ding, Y., and Ren, J.: Classification and Geographical
911 Distribution of Cryosphere, in: *Introduction to Cryospheric Science*. Springer
912 Singapore, Singapore, 33–79, https://doi.org/10.1007/978-981-16-6425-0_2, 2021.

913 Rabatel, A., Ceballos, J. L., Micheletti, N., Jordan, E., Braitmeier, M., González,
914 J., Mölg, N., Ménégoz, M., Huggel, C., and Zemp, M.: Toward an imminent extinction
915 of Colombian glaciers?, *Geografiska Annaler: Series A, Phys Geog*, 100, 75–95,
916 <https://doi.org/10.1080/04353676.2017.1383015>, 2018.

917 Ragettli, S., Immerzeel, W. W., and Pellicciotti, F.: Contrasting climate change
918 impact on river flows from high-altitude catchments in the Himalayan and Andes
919 Mountains, *Proc. Natl. Acad. Sci. U.S.A.*, 113, 9222–9227,
920 <https://doi.org/10.1073/pnas.1606526113>, 2016.

921 Rasul, G., Pasakhala, B., Mishra, A., and Pant, S.: Adaptation to mountain
922 cryosphere change: issues and challenges, *Clim Dev*, 12, 297–309,
923 <https://doi.org/10.1080/17565529.2019.1617099>, 2020.

924 Rosier, S. H. R., Reese, R., Donges, J. F., De Rydt, J., Gudmundsson, G. H., and
925 Winkelmann, R.: The tipping points and early warning indicators for Pine Island Glacier,

926 West Antarctica, *The Cryosphere*, 15, 1501–1516, <https://doi.org/10.5194/tc-15-1501->
927 2021, 2021.

928 Schwank, J., Escobar, R., Girón, G. H., and Morán-Tejeda, E.: Modeling of the
929 Mendoza river watershed as a tool to study climate change impacts on water availability,
930 *Environmental Science & Policy*, 43, 91–97,
931 <https://doi.org/10.1016/j.envsci.2014.01.002>, 2014.

932 Serban, R., Jin, H., Serban, M., and Luo, D.: Shrinking thermokarst lakes and
933 ponds on the northeastern Qinghai-Tibet plateau over the past three decades,
934 *PERMAFROST AND PERIGLACIAL PROCESSES*, 32, 601–617,
935 <https://doi.org/10.1002/ppp.2127>, 2021.

936 Stecher, G., Hohensinner, S., and Herrnegger, M.: Changes in the water retention
937 of mountainous landscapes since the 1820s in the Austrian Alps, *Front. Environ. Sci.*,
938 11, 1219030, <https://doi.org/10.3389/fenvs.2023.1219030>, 2023.

939 Sun, B., Liu, J., Ren, F., Li, H., Zhang, G., Ma, J., Ma, B., and Li, Z.: Effects of
940 seasonal freeze–thaw and wind erosion on runoff and sediment yields of three loamy
941 slopes of Loess Plateau, China, *CATENA*, 215, 106309,
942 <https://doi.org/10.1016/j.catena.2022.106309>, 2022.

943 Tang, G., Clark, M. P., Knoben, W. J. M., Liu, H., Gharari, S., Arnal, L., Beck, H.
944 E., Wood, A. W., Newman, A. J., and Papalexiou, S. M.: The Impact of Meteorological
945 Forcing Uncertainty on Hydrological Modeling: A Global Analysis of Cryosphere
946 Basins, *Water Resour. Res.*, 59, e2022WR033767,
947 <https://doi.org/10.1029/2022WR033767>, 2023.

948 Teng, J., Liu, J., Zhang, S., and Sheng, D.: Frost heave in coarse-grained soils:
949 experimental evidence and numerical modelling, *GEOTECHNIQUE*, 73, 1100–1111,

950 <https://doi.org/10.1680/jgeot.21.00182>, 2022.

951 Teutschbein, C. and Seibert, J.: Bias correction of regional climate model
952 simulations for hydrological climate-change impact studies: Review and evaluation of
953 different methods, *J. Hydrol.*, 456–457, 12–29,
954 <https://doi.org/10.1016/j.jhydrol.2012.05.052>, 2012.

955 Van Der Geest, K. and Van Den Berg, R.: Slow-onset events: a review of the
956 evidence from the IPCC Special Reports on Land, Oceans and Cryosphere, *CURR
957 OPIN ENV SUST*, 50, 109–120, <https://doi.org/10.1016/j.cosust.2021.03.008>, 2021.

958 Vincent, C. and Thibert, E.: Brief communication: Non-linear sensitivity of glacier
959 mass balance to climate attested by temperature-index models, *The Cryosphere*, 17,
960 1989–1995, <https://doi.org/10.5194/tc-17-1989-2023>, 2023.

961 Wang, J., Chen, X., Gao, M., Hu, Q., and Liu, J.: Changes in nonlinearity and
962 stability of streamflow recession characteristics under climate warming in a large
963 glaciated basin of the Tibetan Plateau, *Hydrol. Earth Syst. Sci.*, 26, 3901–3920,
964 <https://doi.org/10.5194/hess-26-3901-2022>, 2022a.

965 Wang, K., Zhang, T., and Clow, G. D.: Permafrost Thermal Responses to
966 Asymmetrical Climate Changes: An Integrated Perspective, *Geophys. Res. Lett.*, 50,
967 e2022GL100327, <https://doi.org/10.1029/2022GL100327>, 2023.

968 Wang, Q., Qi, J., Wu, H., Zeng, Y., Shui, W., Zeng, J., and Zhang, X.: Freeze-Thaw
969 cycle representation alters response of watershed hydrology to future climate change,
970 *CATENA*, 195, <https://doi.org/10.1016/j.catena.2020.104767>, 2020.

971 Wang, S., Yang, Y., and Che, Y.: Global Snow- and Ice-Related Disaster Risk: A
972 Review, *Nat. Hazards Rev.*, 23, 03122002, [https://doi.org/10.1061/\(ASCE\)NH.1527-6996.0000584](https://doi.org/10.1061/(ASCE)NH.1527-6996.0000584), 2022b.

974 Wang, X., Chen, R., Liu, G., Yang, Y., Song, Y., Liu, J., Liu, Z., Han, C., Liu, X.,
975 Guo, S., Wang, L., and Zheng, Q.: Spatial distributions and temporal variations of the
976 near-surface soil freeze state across China under climate change, *Global Planetary*
977 *Change*, 172, 150–158, <https://doi.org/10.1016/j.gloplacha.2018.09.016>, 2019.

978 Wang, Y., Yang, H., Gao, B., Wang, T., Qin, Y., and Yang, D.: Frozen ground
979 degradation may reduce future runoff in the headwaters of an inland river on the
980 northeastern Tibetan Plateau, *J. Hydrol.*, 564, 1153–1164,
981 <https://doi.org/10.1016/j.jhydrol.2018.07.078>, 2018.

982 Wei, L., Zhao, W., Feng, X., Han, C., Li, T., Qi, J., and Li, Y.: Freeze-thaw
983 desertification of alpine meadow in Qilian Mountains and the implications for alpine
984 ecosystem management, *CATENA*, 232, 107471,
985 <https://doi.org/10.1016/j.catena.2023.107471>, 2023.

986 Wen, Y., Liu, B., Jiang, H., Li, T.-Y., Zhang, B., and Wu, W.: Initial soil moisture
987 prewinter affects the freeze–thaw profile dynamics of a Mollisol in Northeast China,
988 *CATENA*, 234, 107648, <https://doi.org/10.1016/j.catena.2023.107648>, 2024.

989 Wiersma, P., Aerts, J., Zekollari, H., Hrachowitz, M., Drost, N., Huss, M.,
990 Sutanudjaja, E. H., and Hut, R.: Coupling a global glacier model to a global
991 hydrological model prevents underestimation of glacier runoff, *Hydrol. Earth Syst. Sci.*,
992 26, 5971–5986, <https://doi.org/10.5194/hess-26-5971-2022>, 2022.

993 Xing, Z. P., Zhao, L., Fan, L., Hu, G. J., Zou, D. F., Wang, C., Liu, S. C., Du, E. J.,
994 Xiao, Y., Li, R., Liu, G. Y., Qiao, Y. P., and Shi, J. Z.: Changes in the ground surface
995 temperature in permafrost regions along the Qinghai–Tibet engineering corridor from
996 1900 to 2014: A modified assessment of CMIP6, *Advances in Climate Change Research*,
997 14, 85–96, <https://doi.org/10.1016/j.accre.2023.01.007>, 2023.

998 Xu, P., Yan, D., Weng, B., Bian, J., Wu, C., and Wang, H.: Evolution trends and
999 driving factors of groundwater storage, recharge, and discharge in the Qinghai-Tibet
1000 Plateau: Study progress and challenges, *Journal of Hydrology*, 631, 130815,
1001 <https://doi.org/10.1016/j.jhydrol.2024.130815>, 2024.

1002 Yang, M., Li, Z., Anjum, M. N., Kayastha, R., Kayastha, R. B., Rai, M., Zhang,
1003 X., and Xu, C.: Projection of Streamflow Changes Under CMIP6 Scenarios in the
1004 Urumqi River Head Watershed, Tianshan Mountain, China, *Front. Earth Sci.*, 10,
1005 857854, <https://doi.org/10.3389/feart.2022.857854>, 2022.

1006 Yao, T., Bolch, T., Chen, D., Gao, J., Immerzeel, W., Piao, S., Su, F., Thompson,
1007 L., Wada, Y., Wang, L., Wang, T., Wu, G., Xu, B., Yang, W., Zhang, G., Zhao, P., 2022.
1008 The imbalance of the Asian water tower. *NATURE REVIEWS EARTH &*
1009 *ENVIRONMENT* 3, 618–632. <https://doi.org/10.1038/s43017-022-00299-4>

1010 Yao, Y., Zheng, C., Andrews, C. B., Scanlon, B. R., Kuang, X., Zeng, Z., Jeong,
1011 S.-J., Lancia, M., Wu, Y., and Li, G.: Role of Groundwater in Sustaining Northern
1012 Himalayan Rivers, *Geophys. Res. Lett.*, 48, <https://doi.org/10.1029/2020GL092354>,
1013 2021.

1014 Yin, G.-A., Niu, F.-J., Lin, Z.-J., Luo, J., and Liu, M.-H.: Data-driven
1015 spatiotemporal projections of shallow permafrost based on CMIP6 across the Qinghai–
1016 Tibet Plateau at 1 km² scale, *Advances in Climate Change Research*, 12, 814–827,
1017 <https://doi.org/10.1016/j.accre.2021.08.009>, 2021

1018 Zekollari, H., Huss, M., Farinotti, D., and Lhermitte, S.: Ice - Dynamical Glacier
1019 Evolution Modeling—A Review, *Reviews of Geophysics*, 60, e2021RG000754,
1020 <https://doi.org/10.1029/2021RG000754>, 2022.

1021 Zhang, T.: Influence of the seasonal snow cover on the ground thermal regime: An

1022 overview, *Reviews of Geophysics*, 43, 2004RG000157,
1023 <https://doi.org/10.1029/2004RG000157>, 2005.

1024 Zhang, S., Gao, X., Zhang, X., and Hagemann, S.: Projection of glacier runoff in
1025 Yarkant River basin and Beida River basin, Western China, *Hydrol. Process.*, 26, 2773–
1026 2781, <https://doi.org/10.1002/hyp.8373>, 2012.

1027 Zhang, T., Li, D., and Lu, X.: Response of runoff components to climate change
1028 in the source-region of the Yellow River on the Tibetan plateau, *Hydrol. Process.*, 36,
1029 <https://doi.org/10.1002/hyp.14633>, 2022.

1030 Zhang, Z., Wang, Y., Ma, Z., and Lv, M.: Response mechanism of soil structural
1031 heterogeneity in permafrost active layer to freeze-thaw action and vegetation
1032 degradation, *CATENA*, 230, <https://doi.org/10.1016/j.catena.2023.107250>, 2023.

1033 Zhang, Y. and Ma, N.: Spatiotemporal variability of snow cover and snow water
1034 equivalent in the last three decades over Eurasia, *Journal of Hydrology*, 559, 238–251,
1035 <https://doi.org/10.1016/j.jhydrol.2018.02.031>, 2018.

1036 Zhu, Y. Y. and Yang, S.: Evaluation of CMIP6 for historical temperature and
1037 precipitation over the Tibetan Plateau and its comparison with CMIP5, *Advances in*
1038 *Climate Change Research*, 11, 239–251, <https://doi.org/10.1016/j.accre.2020.08.001>,
1039 2020.